

UNCLASSIFIED

AD **409 162**

DEFENSE DOCUMENTATION CENTER

FOR

SCIENTIFIC AND TECHNICAL INFORMATION

CAMERON STATION, ALEXANDRIA, VIRGINIA



UNCLASSIFIED

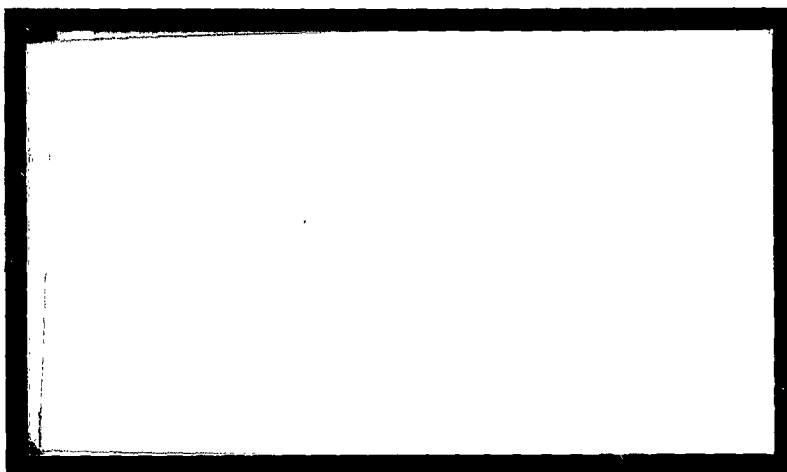
NOTICE: When government or other drawings, specifications or other data are used for any purpose other than in connection with a definitely related government procurement operation, the U. S. Government thereby incurs no responsibility, nor any obligation whatsoever; and the fact that the Government may have formulated, furnished, or in any way supplied the said drawings, specifications, or other data is not to be regarded by implication or otherwise as in any manner licensing the holder or any other person or corporation, or conveying any rights or permission to manufacture, use or sell any patented invention that may in any way be related thereto.

N-63-4-2

University of Utah

Department of Chemical Engineering

CATALOGED BY DDC
AS AD No. 409162



409162



Salt Lake City, Utah

DESIGN AND CONSTRUCTION OF MULTI-RING APPARATUS FOR
USE AT HIGH PRESSURES, FORCE DISTRIBUTION BY
MEANS OF THE IRREVERSIBLE COMPRESSIBILITY
OF SILICA GLASS, AND THE EFFECT OF PRES-
SURE ON ORBITAL ELECTRON CAPTURE

by

W. B. Gogarty, S. S. Kistler, and E. B. Christiansen

Technical Report VII, June 1963

Office of Naval Research

Contract No. 1288(02), Project No. NR-052-357

University of Utah College of Engineering

Department of Chemical Engineering

Salt Lake City 12, Utah

(Reproduction in whole or in part is permitted for any purpose
of the United States Government.)

TABLE OF CONTENTS

	<u>Page</u>
List of Figures and Tables	ii
SECTION I: DESIGN AND CONSTRUCTION OF MULTI-RING APPARATUS FOR USE AT HIGH PRESSURES	1
Abstract	1
Introduction	2
The Anvil Assembly	3
Fabrication of the Anvil Assembly	9
Tables	12
Figures	14
Literature Cited	15
SECTION II: IRREVERSIBLE COMPRESSIBILITY OF SILICA GLASS AS A MEANS OF DETERMINING THE DISTRIBUTION OF FORCE IN HIGH-PRESSURE CELLS	16
Abstract	16
Introduction	16
Theoretical Considerations of Force Distribution over Type I Pressure Cell	16
Theoretical Considerations of Force Distribution over Type II Pressure Cell	21
Experimental Determinations of Force Distribution over Type II Pressure Cell	23
Tables	27
Figures	31
Literature Cited	33
SECTION III: THE EFFECT OF PRESSURE ON ORBITAL ELECTRON CAPTURE	34
Abstract	34
Introduction	35
Selection of Radioactive Isotopes	37
Pressure Cells	37
Pressure Equipment	38
Radioactive Counting	39
Sample Preparation	45
Counting Geometry	46
Results	47
Discussion	47
Conclusions	50
Tables	52
Figures	57
Literature Cited	65
Distribution List	66

LIST OF FIGURES AND TABLES

<u>SECTION I:</u>	<u>Tables</u>	<u>Page</u>
External Support on a 1-inch Anvil with an Assembly Diameter of 3 Inches		12
Values of the Different Radii for a 3-Ring Anvil Assembly		12
Radial Deformations in a 3-Ring Assembly		13
Interferences for a 3-Ring Assembly		13
	<u>Figures</u>	
Schematic Diagram of Anvil Assembly		14
Arrangement of Rings and Anvil for Determining the Values of Interference to be Obtained on Assembly		14
 <u>SECTION II:</u>	 <u>Tables</u>	
Experimental Data for Silica Glass		27
Effect of Center-section Thickness on Blowout in Silver Chloride-Modified Type II Pressure Cell		29
Comparison of Measured and Calculated Values of Force		29
Influence of Time of Pressurization		30
	<u>Figures</u>	
Pressure Cells on Bottom Anvil before Compression		31
Schematic Diagram of Anvil Assembly		31
Crushed Glass Disk showing Method of Sampling		31
Density Profile of a Symmetrically Loaded Disk, with Approximately Equal Area Samples taken 180° Apart		31
Density Profile of a Symmetrically Loaded Disk, with Unequal Area Samples taken 180° Apart		31
Density Profile of an Unsymmetrically Loaded Disk		32
Data Based on Area Mean Density and Average Pressure with Preliminary Curve Used in Determining the Unit Pressures on Incremental Areas		32
Percentage Change in Density versus Pressure for Silica Glass		32
 <u>SECTION III:</u>	 <u>Tables</u>	
Cell Dimensions		52
Summary of Data from Test on Operation of the Counting Equipment		53
Data and Results for Be ⁷ in the Lead-Modified Type II Pressure Cell		54
Data and results for Be ⁷ in the Type I Pressure Cell		55
Data and Results for Ba ¹³¹ in the Silver Chloride-Modified Type II Pressure Cell		55
Effect on the Counting Ratio by Spreading a Pressure Cell		56

<u>Figures</u>	<u>Page</u>
Cross-sectional Details of Pressure Cells before Force has been Applied .	57
Schematic Diagram of the Anvil Assembly	58
Change in the Final Ratio/Initial Ratio with Time for Be ⁷ in the Lead-Modified Type II Pressure Cell	59
Change in the Final Ratio/Initial Ratio with Time for Be ⁷ in the Type I Pressure Cell	60
Change in the Final Ratio/Initial Ratio with Time for Ba ¹³¹ in the Silver Chloride-Modified Type II Pressure Cell	61
Fractional Increase in the Total Decay Constant with Pressure for Be ⁷ in the Lead-Modified Type II Pressure Cell	62
Fractional Increase in the Total Decay Constant with Average Pressure for Be ⁷ in the Type I Pressure Cell	63
Fractional Increase in the Total Decay Constant with Pressure for Ba ¹³¹ in the Silver Chloride-Modified Type II Pressure Cell	64

SECTION I

DESIGN AND CONSTRUCTION OF MULTI-RING APPARATUS FOR USE AT HIGH PRESSURES

(W. B. Gogarty, S. S. Kistler, and E. B. Christiansen)

ABSTRACT

A derivation is presented of equations which can be used in the design of high pressure apparatus utilizing multi-ring support. The use of these equations is illustrated by the design calculation for a multi-ring apparatus known as the anvil assembly. The particular assembly described uses three rings for external support. This assembly is capable of developing average pressures of 160,000 atm for minimum periods of two weeks. The methods and materials used in the fabrication of the assembly are also presented.

INTRODUCTION

Experimentation in the field of extremely high pressures is generally performed by making use of pressure equipment which consists of a hydraulic press and an apparatus which will concentrate a large force on a small area. This study is concerned with the latter which, of necessity, must be designed and constructed to utilize efficiently materials with highest available strengths. Several examples of such devices have been described [2,4].

Applications with different types of high strength apparatus have been described in the literature [2,4]. Design equations for apparatus utilizing multi-ring support were derived in this paper for a multi-ring apparatus illustrated in Figure 1 and known as an anvil assembly. However the methods employed in the derivation are general. The derivation of these equations is performed for a class of multi-ring apparatus known as the anvil assembly. Methods applied in the derivation, however, are general. The use of these equations is illustrated with design calculations for a particular anvil assembly. This anvil assembly, when constructed in accordance with the methods outlined below, is capable of developing average pressures of 160,000 atm for a minimum period of two weeks or 100,000 atm for a period greater than two months.

NATURE OF THE ANVIL ASSEMBLY

Component parts of the anvil assembly are shown in Figure 1* The central portions of this assembly, listed as B in Figure 1, are called anvils, and an identical conical angle α_0 is ground on each of these anvils to give the desired strength and flat working surface. The outer portions of this assembly, listed as A in Figure 1, represent one or more steel rings which furnish external support to the anvils. High average pressures are developed between the flat surfaces of the anvils by forcing the two portions of the assembly together with a hydraulic press. The upper limit of the average pressure developed by the anvil assembly is determined by:

1. the magnitude of the flat working area of the anvils;
2. the value of the conical angle;
3. the amount of external support furnished the anvils;
4. the method and materials of the construction.

DESIGN EQUATIONS

Lamé and Clapeyron [5] were the first to obtain equations for the design of thick-walled cylinders. The expressions developed by these authors for internal pressure and radial deformation are:

$$p_i = \frac{\sigma_t (b^2 - a^2) + 2b^2 p_o}{a^2 + b^2} \quad (1)$$

$$u = \left(\frac{1 - \mu}{E} \right) \frac{a^2 p_i - b^2 p_o}{b^2 - a^2} \frac{1}{r} + \left(\frac{1 + \mu}{E} \right) \frac{a^2 b^2 (p_i - p_o)}{(b^2 - a^2) \bar{r}}, \quad (2)$$

where a = internal ring radius (in.), b = external ring radius (in.),
 E = modulus of elasticity (psi), p_o = external pressure on the ring (psi),
 \bar{r} = variable radius between a and b (in.), μ = Poisson's ratio (in./in), and
 σ_t = maximum tangential stress at the inner radius of the cylinder (psi).
 These equations were obtained on the premise that materials are not stressed beyond their elastic limit.

*Figures for Section I are found on p. 14.

Design calculations for an anvil assembly in which one ring furnishes the external support can be made directly by using Equations (1) and (2). In the usual case, the modulus of elasticity of the anvil material will be greater than that of the support ring. Thus, in using these equations an anvil under no load can be taken as completely rigid with respect to its support ring.

For an assembly with a single ring, Equation (1) shows that the support given an anvil under no load cannot be made greater than the maximum tangential stress of the supporting steel even with a ring of infinite thickness. However, the support to the anvil can be increased above the value of the maximum tangential stress either by causing an effect analogous to auto-fretting or by use of multi-ring support.

The process of auto-fretting is performed by making the interference for assembly between the anvil and the support ring of such a value that the inner fibers are stressed beyond their elastic limit. Unfortunately, the determination of the amount that external support is increased by this process is at best a trial and error procedure. In addition, the size of the supporting ring renders almost impossible the obtaining of a uniformly hardened ring by the process of heat treating. The use of multi-ring support, on the other hand, permits the thickness of the individual rings to be kept small, and the chance of obtaining a more homogeneously hardened steel ring by heat treating is greatly enhanced. Also, the design equations derived in the following paragraphs can be used to determine the external support furnished the anvil in the multi-ring assembly.

The use of multi-ring support in design necessitates a condition for establishing the dimensions of individual rings so that the most effective use of materials is obtained. This design condition is inferred by Seely and Smith [6] for their two-ring pressure vessel in which the ratio of the outside-to-inside radius of both rings is made constant. The extension of this condition to a multi-ring assembly makes possible the determination of the radii of any ring in the assembly by

$$\begin{aligned} r_1 &= r_1 & r_4 &= m^3 r_1 \\ r_2 &= m r_1 & r_5 &= m^4 r_1, \text{ etc.}, \\ r_3 &= m^2 r_1 & & \end{aligned} \quad (3)$$

where m is a constant determined by the inside radius, r_1 , of the smallest ring and by the outside radius of the largest ring.

By utilizing the condition of Equation (3), general design equations for multi-ring assemblies can be derived by using Equations (1) and (2). For a multi-ring assembly with dimensions satisfying Equation (3) and containing j rings, Equation (1) can be written for any ring as

$$p_i = \frac{\sigma_t (m^2 - 1) + 2m^2 p_o}{m^2 + 1} \quad (4)$$

For the outermost ring, p_o can be taken as zero since one atmosphere is usually small compared to the pressures developed between the ring boundaries. With zero pressure on the outside surface of the outermost ring, the internal pressure on this ring becomes

$$(p_i)_1 = \frac{\sigma_t (m^2 - 1)}{m^2 + 1}, \quad (5)$$

where the subscript on p_i refers to the outermost ring. Since the inside surface of the outermost ring is in contact with the outside surface of the second outermost ring, the pressure at this position will be equal. The value of internal pressure from Equation (5) can therefore be substituted for the value of p_o in Equation (4) to yield an equation for determining the internal pressure on the second outermost ring. This equation is

$$(p_i)_2 = \frac{\sigma_t (m^2 - 1)}{m^2 + 1} \left[1 + \frac{2m^2}{m^2 + 1} \right]. \quad (6)$$

The condition of equal pressure will hold for all ring boundaries in the assembly. Therefore, Equation (6) can also be substituted into Equation (4) for the value of p_o so that an equation for the internal pressure on the third outermost ring is obtained. If this procedure of repeatedly substituting for p_o in Equation (4) is continued until ring j is reached, the resulting equation will be a geometric progression.

The sum of this progression gives the internal pressure on ring j as

$$(p_i)_j = \sigma_t \left[\left(\frac{2m^2}{m^2 + 1} \right)^j - 1 \right]. \quad (7)$$

Design calculations are facilitated when numbering of the rings in the assembly starts with the innermost ring and proceeds outward. With this type of numbering, the exponent in Equation (7) can be adjusted in terms of the total number of rings, T , and the ring numbered f . With this adjustment, the internal pressure on ring f becomes

$$(p_i)_f = \sigma_t \left[\left(\frac{2m^2}{m^2 + 1} \right)^{T - f + 1} - 1 \right] \quad (8)$$

and the external pressure on ring f becomes

$$(p_o)_f = \sigma_t \left[\left(\frac{2m^2}{m^2 + 1} \right)^{T - f} - 1 \right]. \quad (9)$$

By using Equation (8) to calculate the external support furnished an anvil, one can determine the increase in support as more rings are used in an assembly of constant outside diameter. Results for this type of calculation are presented in Table I. Calculations for this table were made by using 150,000 psi as the value for the maximum tangential stress of the steel rings.

If the condition given by Equation (3) is used in connection with Equation (2), the radial deformation at a radius \bar{r} for any ring in the assembly becomes

$$u = \frac{1}{E(m^2 - 1)} \left[\bar{r}(1 - \mu) (p_i - m^2 p_o) + \frac{b^2}{\bar{r}} (1 + \mu) (p_i - p_o) \right]. \quad (10)$$

By using the radius a in Equation (10), together with the internal and external pressures from Equations (8) and (9), the internal radial deformation of ring f is furnished by

$$(u_{i f}) = \frac{\sigma_t a}{E(m^2 - 1)} \left\{ (1 - \mu) \left[\left(\frac{2m^2}{m^2 + 1} \right)^{T - f + 1} - 1 + m^2 - m^2 \left(\frac{2m^2}{m^2 + 1} \right)^{T - f} \right] + (1 + \mu) m^2 \left[\left(\frac{2m^2}{m^2 + 1} \right)^{T - f + 1} - \left(\frac{2m^2}{m^2 + 1} \right)^{T - f} \right] \right\} \quad (11)$$

In a similar manner, the external radial deformation of ring f is

$$(u_{o f}) = \frac{\sigma_t b}{E(m^2 - 1)} \left\{ (1 - \mu) \left[\left(\frac{2m^2}{m^2 + 1} \right)^{T - f + 1} - 1 + m^2 - m^2 \left(\frac{2m^2}{m^2 + 1} \right)^{T - f} \right] + (1 + \mu) \left[\left(\frac{2m^2}{m^2 + 1} \right)^{T - f + 1} - \left(\frac{2m^2}{m^2 + 1} \right)^{T - f} \right] \right\} \quad (12)$$

DESIGN CALCULATIONS

The usefulness of the equations derived in the last section is best illustrated by presenting the methods used in designing a particular anvil assembly. This anvil assembly, for which the design information is presented, has, for example, been tested repeatedly at average pressures of 160,000 and 100,000 atm for periods of two weeks and two months, respectively. The methods used in the fabrication of this particular assembly are given in the last section of the paper.

In this design, rings are to be specified to support a 1 in. x 1 in. cylindrical anvil manufactured of cemented tungsten carbide, grade K-96, by Kennametal, Inc., of Latrobe, Pennsylvania. Grade Alco S steel manufactured by Universal Cyclops Company was selected as the material from which to construct the support rings. The modulus of elasticity of the carbide is given by the manufacturer as 94×10^6 psi, as compared to a modulus of 30×10^6 for the steel [1]. The difference in these two moduli permitted the use of the assumption, as discussed above, that anvils under no load are rigid with respect to steel rings. The Alco S steel was used with a hardness of Rockwell 50 on the "C" scale which gives a proportional limit of 167,000 psi [1]. Poisson's ratio was taken as 0.28 for the Alco S. steel.

Theoretically, the initial phase in designing an anvil assembly should begin with the determination of the external support needed by the anvil under no axial loading so that radial fractures will not occur in the anvils after the maximum load has been applied. This determined external support can then be used in Equation (8) as the value of pressure between the innermost ring and the anvil, and a combination of the three remaining variables can be selected to satisfy the equation.

Unfortunately, mathematical relationships were not available for calculating the external support required by the anvil assembly so the initial design phase could not be accomplished by the straightforward method described above. The alternate method used was to calculate the amount of external support furnished a 1-inch carbide anvil as a function of the total number of rings for various outside assembly diameters. These calculations were made by using Equation (8) with the value of the maximum tangential stress fixed for the Alco S steel at 150,000 psi. The maximum tangential stress was placed at this value to assure that lateral expansion of the anvils under axial load would not cause the innermost fibers of the steel rings to exceed their proportional limit. For each outside assembly diameter, a set of results was obtained similar to those presented in Table I. These results were then compared in order to select an outside assembly diameter and the total number of rings. The selection was based on considerations of manufacturing costs and desired maximum support. An assembly containing three rings with an overall outside diameter of three inches was selected. The values of the four radii for this assembly were then calculated by using Equation (3). These radii are tabulated in Table II. By using Equation (11) for the inside radius and Equation (12) for the outside radius, the amount of radial deformation for the three rings was determined to be as presented in Table III. In order to obtain maximum support from the rings without exceeding the maximum tangential stress, the rings had to be fabricated so that when the assembly was complete, all radial deformations listed in Table III would be realized. This was accomplished by allowing for the values of interference listed in Table IV.

The final phase in the anvil assembly design consisted of determining an appropriate conical angle for the anvils. This angle was fixed at four degrees for the particular anvil assembly being discussed. This choice was

based on results of experiments performed to determine the time that the assembly would withstand maximum pressure without failure.

FABRICATION OF THE ANVIL ASSEMBLY

Fabrication of the anvil assembly, the design details of which are presented in the preceding section, began with the preparation of the steel support rings. The required number of disks, approximately 1-inch thick, were cut from three pieces of Alco S bar stock with appropriate diameters. By use of the lathe, rings of three sizes were formed which had oversized outside diameters and undersized inside diameters within about 0.050 of an inch of the values listed in Table II. This extra material was left on the rings so that any decarburization or warping that might occur during heat treating could be removed in the final grinding operations.

The process of hardening the Alco S steel rings was started by heating to 1750° F, the temperature required for quenching. Decarburization was minimized at this high temperature by placing the rings in a closed container and surrounding them with elemental carbon. Time in the furnace at these high temperatures was reduced by allowing the furnace to reach 1400° F before the rings were inserted and then by removing the rings for oil quenching as soon as the furnace temperature rose to 1750° F. Rings were left in the container while they were moved to the oil quenching bath so that the heat loss by radiation would be decreased. After the rings had been hardened by the oil quench, the temperature of the furnace was reduced to 1000° F, and the cold rings were inserted for annealing. The container and carbon were not used for annealing since the rate of decarburization became negligible at this lower temperature. The cold rings reduced the temperature of the furnace so that an annealing time of two hours was measured from the time that the furnace regained the original 1000° F. Tests on a hardness-testing machine verified the fact that rings heat treated in accordance with the above method invariably had a Rockwell hardness of 50 on the "C" scale.

Two methods of assembly are presently specified on mechanical designs of equipment requiring interference fits. One method utilizes heating and cooling of the component parts so that the corresponding expansion and contraction will allow assembly. With the other method, interference tapers are ground on

mating parts so that they can be forced together to give the desired radial deformation. In order to use the first method of assembly for the rings, the heating necessary to obtain the correct amount of expansion had to be of such a nature that the hardness of the steel was not affected. Since the required heating affected the degree of hardness, the second method of assembly was used. Therefore, after heat-treating had been completed, the flat surfaces of the rings were surface ground to give the desired height, and the inner and outer radial surfaces of each ring were ground to a taper of 1/8-inch/foot. The solid carbide cylinder was ground on the lathe to the same taper. A tool post grinder with a diamond wheel was used in this operation.

Values of interference specified in Table IV had to be obtained upon assembly of the component parts. Higher values of interference than those specified caused the rings to fracture when the assembly was made. With lower values, the external support on the carbide anvils was insufficient to prevent radial fracturing. In order to obtain the correct values for the interference, a gauging method was used whereby the vertical projection of each ring and anvil was measured with respect to another ring before assembly. The arrangement used to gauge the rings and anvil before assembly is shown in Figure 2. Values for the vertical projections in Figure 2 were calculated by using the value of the taper ground on the rings and anvils in connection with the values of interference listed in Table IV.

Owing to the fact that under an axial load the greatest increase in stress occurs at the inner radius of the inner ring of the assembly, it was found desirable to increase the value of the proportional limit of the steel at this point by the process of auto-frettaging. This strengthening process was applied to the inner ring by overstressing the inner fibers on a hardened steel mandrel ground with the same taper as the rings. These inner rings were placed on the mandrel while the i.d. was still 0.010 inches under size and forced down the mandrel for a distance of one inch, a process which overstressed the inner fibers. These rings were then removed and ground to the final dimension for assembly.

Assembly of the solid core and rings was accomplished by lubricating all surfaces and molybdenum sulfide, used as an extremely fine powder suspended in a volatile solvent. All rings and anvils were pressed together in a

30-ton press at one operation. Care had to be exercised during this operation as outer rings sometimes failed and were shot from the assembly. Also, outer rings were observed to fail for a period of as long as four hours after pressing. Therefore, final machining operations were not performed on rings until at least this period of time had elapsed.

The final machining operation consisted of making a fine cut with the diamond wheel on both ends of the solid carbide core to ensure parallel surfaces and then of cutting the four-degree conical angle to give the desired diameter for the flat working surface.

Anvil assemblies in which anvils fractured after long periods of operation were not discarded but were refinished. Refinishing was accomplished by first grinding the steel of the rings below that portion of the anvil which had fractured. The anvil was then resurfaced, and a new conical angle was ground. All grinding operations in the refinishing process were performed on the lathe, the tool post grinder being used. These refinishing operations were continued after fracturing until either unit of the anvil assembly was ground below a height of 0.40 inches. Units below this height would not support a high total thrust and were therefore discarded.

TABLE I
EXTERNAL SUPPORT ON A 1-INCH ANVIL WITH AN
ASSEMBLY DIAMETER OF 3 INCHES

Number of Rings	o.d./i.d. (b/a)	External Support (psi)
1	3.00	1.20×10^5
2	1.73	1.88×10^5
3	1.44	2.22×10^5
4	1.32	2.40×10^5
7	1.17	2.67×10^5
10	1.12	2.76×10^5

TABLE II
VALUES OF THE DIFFERENT RADII FOR A 3-RING ANVIL ASSEMBLY

Radius	Value (in.)
r_1	0.50
r_2	0.72
r_3	1.04
r_4	1.50

TABLE III
 RADIAL DEFORMATIONS IN A 3-RING ASSEMBLY

Ring number	Internal radial deformation (in. $\times 10^3$)	External radial deformation (in. $\times 10^3$)
I	3.48	2.11
II	4.46	3.28
III	5.73	2.45

TABLE IV
 INTERFERENCES FOR A 3-RING ASSEMBLY

Boundary	Interference (in. $\times 10^3$)
Solid core-Ring I	6.96
Ring I-Ring II	4.70
Ring II-Ring III	4.90

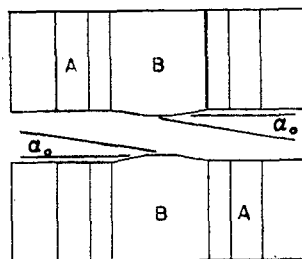


Fig. 1. Schematic diagram of anvil assembly.

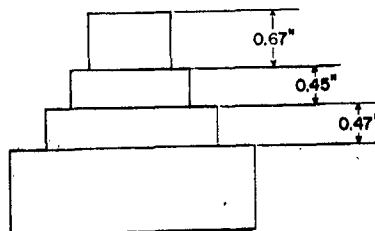


Fig. 2. Arrangement of rings and anvil for determining the values of interference to be obtained on assembly.

LITERATURE CITED

1. Boyd, William A. and S. S. Kistler, "A Study of Thick-Walled Cylinders as Tensile Members for High Pressure Vessels, With Particular Attention to Steels and Their Heat Treatment for Maximum Performance", Technical Report III, ONR Contract No. 1288(02) Project No. NR-052-357, University of Utah College of Engineering (March, 1958).
2. Bridgman, P. W., Proc. Am. Acad. Arts Sci., 81, 165 (1952).
3. Fitch, R. A., T. E. Slykhouse, and H. G. Drickamer, J. Opt. Soc. Am., 47, 1015 (1957).
4. Hall. H. T., Rev. Sci. Instr., 29, 267 (1958).
5. Lamé, G. and B. P. E. Clapeyron, Memoires Presentes Par Divers Savans, 4 (1833).
6. Seely, F. B. and J. O. Smith, Advanced Mechanics of Materials, John Wiley and Sons, Inc., New York (1952).

SECTION II

IRREVERSIBLE COMPRESSIBILITY OF SILICA GLASS AS A MEANS OF DETERMINING THE DISTRIBUTION OF FORCE IN HIGH-PRESSURE CELLS

(W. B. Gogarty, S. S. Kistler, and E. B. Christiansen)

ABSTRACT

The theoretical distribution of force over two types of cells used at pressures up to 160,000 atm is considered and compared with experimental results obtained by using silica glass as a pressure indicator. Experimental data for the pressure-irreversible density-change relation of silica glass to pressures of 200,000 atm are reported. Differences between results of the present investigation and those of previous investigations are discussed.

INTRODUCTION

In an experimental investigation to determine the effect of pressure on radioactive decay by orbital electron capture (see Section III), the three pressure cells shown in Figure 1* were employed. These cells were compressed between anvils supported with hardened steel rings to generate average pressures up to 160,000 atm. The anvils and supporting rings are shown in Figure 2, as parts B and A, respectively. Methods used in the design and fabrication of the anvil assembly are discussed in Section I and elsewhere. [5, 6]

A major problem encountered with this type of anvil assembly is the determination of the force distribution over a particular type of pressure cell. An investigation therefore was initiated to obtain the approximate force distributions over the cells used in the radioactive decay studies.

THEORETICAL CONSIDERATIONS OF FORCE DISTRIBUTION OVER TYPE I PRESSURE CELL

As the flat surfaces of the anvils come together on the Type I pressure cell (see Figure 1), the two pipestone disks are forced together and the entire cell approximates a solid disk. The first attempt to analyze the force distribution over such a solid disk was made by Bridgman in connection with his studies on the effect of shearing stress on materials at high pressures. [1] A more recent analysis of this problem has been made by Komkov. [8]

In making his analysis, Bridgman assumed that both surfaces of the anvils approximated semi-infinite planes, with the disk acting as a cylinder and

*Figures for Section II are found on pp. 31-32.

applying a certain force distribution to both of these surfaces. With this assumption, Hertz's equation [9] could be used to give the normal deformation of the surfaces as

$$w = \frac{\alpha + 2\delta}{4\pi\delta(\alpha + \delta)} \phi \quad (1)$$

where α and δ are constants defined in terms of the modulus of elasticity and Poisson's ratio and ϕ is a function which depends on the pressure distribution and position. The difference in deformation between the center and outside edge of the anvil surfaces was then calculated with equation (1) by assuming a uniform pressure distribution. The results of this calculation indicated that after pressing, disks should appear as double convex lenses. Disks after pressing were found by Bridgman to be lenticular in shape; this observation, together with the fact that the use of a uniform pressure distribution in Hertz's equation had led to a prediction of this shape, caused Bridgman [2] to assume, as an approximation of the first order, that the force over the disk was uniformly distributed. As an approximation of the second order, the pressure on the disk in an annular ring was assumed by Bridgman to be greater than that at the center or the edge; but the difference in pressure between the annular ring and the center or the edge was thought to be small.

These early calculations and experimental observations by Bridgman [1,2] seemed to have set the precedent in the field of high pressure for the determination of the force distribution over this type of pressure cell. Hence, present-day investigators still report pressures in terms of total thrust divided by cross-sectional areas with the implication that this average pressure is close to the pressure developed in the cell. That the average pressure is not approached in this type of cell can be seen from the following experimental results.

EXPERIMENTAL DETERMINATIONS OF FORCE DISTRIBUTION OVER TYPE I PRESSURE CELL

Bridgman and Simon [3] reported that silica glass under pressure shows a permanent change in density when the pressure applied exceeds 100,000 atm. Values of pressure given by these investigators were calculated by dividing the total force applied to a glass disk by its final area. They mentioned that above 100,000 atm small fragments from the outer rings of the glass disks showed permanent increases in density as high as 17%. Central portions of the glass disks were reported as showing only a maximum increase in density of 7.5%. Although these investigators did not mention the possibility of nonuniform force

distribution over the anvil surfaces, the great difference in density change for a given disk indicated that outer portions of the glass disks were taking a disproportionate fraction of the total load. Thus, the problem of force distribution in the Type I cell was approached with the idea that measured variations in density across a silica glass disk would approximate the force distribution in the cell.

To make accurate measurements of the density of any small portion of a crushed glass disk or of the entire disk, a sink-float technique was developed. For this method of measurement, mixtures of bromobenzene (1.50 g per ml) and s-tetrabromoethane (2.96 g per ml) were used in glass-stoppered volumetric flasks held at a constant temperature in a closely controlled bath. Fragments of glass were dropped into the flasks filled with mixtures of the liquids having densities slightly lower than those anticipated for the fragments. S-tetrabromoethane was added dropwise to each flask accompanied with thorough mixing until the fragments neither settled nor rose. This technique was very sensitive, and the influence of one or two drops of s-tetrabromoethane in 50 ml of the mixture could easily be observed. After the composition having the same density as that of the glass fragments was found, the liquid was collected in a pycnometer after passing through a fine screen to capture the fragments. The pycnometer was then placed inside the bath, and the liquid density was determined by conventional means. Densities with an accuracy of four significant figures were obtained by this method.

Glass disks from the pressure apparatus were crazed or cracked and appeared to be white. When samples from approximately 90% of the material in a disk were dropped into the specific gravity liquid, they became clear owing to the displacement of the air. Samples from the other 10% of the material remained white after being placed in liquid. The material which remained white was always found in the outermost ring of a disk. To determine the amount of error associated with the entrapment of air in samples from the outermost ring of a disk, a sample appearing white in the specific gravity liquid was boiled until it became 100% transparent. The density of the transparent sample was found to be identical with the value of density determined before the air had been removed by boiling. These identical values of density indicated that the error in density caused by entrapped air was insignificant for samples which remained white after being placed in the specific gravity liquid.

The pressure apparatus for the glass experiments consisted of an anvil assembly of the type shown in Figure 2, the total thrust being supplied by a 50-ton press. The flat surfaces of the anvils were 0.5 in. in diameter, and the glass disks placed between the anvils were 0.24 in. in diameter and approximately 0.006 in. thick. A lead ring 0.004 in. thick and with an outside diameter of 1/2 in. was placed around each disk of glass before pressurization. This ring served to center the disk by means of a jig and also helped to contain the glass fragments around the outside of the disk after pressurization.

Initial experiments showed that very slight departure of the anvil surfaces from the parallel caused one side of the glass disk to be much more extensively compressed than the other. This difficulty was overcome by rigging a tool-post grinder on the lower platen of the press and by grinding both anvil surfaces in situ. The roughened surface of a freshly ground anvil tended to crack the glass and to produce irregular loading. Consequently, the anvil surfaces were polished with diamond paste until a mirrorlike finish had been obtained on both surfaces. Only with anvils prepared in this way was it possible to obtain a symmetrical and reproducible compression of the glass disks.

A great deal of time was spent trying to prepare glass disks with the surfaces flat, smooth, and parallel. Metallographic techniques were adequate to prepare single surfaces with the desired flatness and smoothness, but the control for keeping the surfaces of the disks parallel was not satisfactory. A grinding technique for forming the disks on the lathe was finally developed whereby the surfaces of disks were made parallel to within 0.0001 in. Details of the grinding process used are described in Section I and elsewhere [5, 6].

After a disk was completed and positioned on the lower anvil, it was pressurized at a low rate. Total thrust on the disk was calculated from the area of the press cylinder and the oil pressure. All the earlier measurements were made with a dwell time of 1 minute whereas later measurements were made with longer dwell times. Rapid reduction of pressure often resulted in a "blowout" of the disk. It was surmised that a slow rate of pressure reduction was conducive to relieving the stresses built up in the metal anvils and glass disks. All pressing operations were performed at a temperature of approximately 75° F.

Compressed disks were sampled so that the variation in density over the whole disk could be determined. Two opposing sections from the outer ring, which was usually loose from the center of the disk, were always selected in the sampling. These sections were labeled a and b in Figure 3. Inside this ring the remaining center section was sectioned approximately along the dotted lines, as shown in Figure 3, and the two outer portions labeled c and d were discarded. The central portion was divided into as many as five parts along the diameter. The radial lengths of samples from a disk were measured with a traveling microscope. Each sample was then transferred to a float-sink bottle, and the densities of all samples were carefully determined.

With the traveling microscope measurements, two different sets of incremental areas were calculated, the total area of the disk being represented by each set. These two sets of incremental areas were based on the radial lengths of samples determined in opposite directions from the center of the disk. Incremental calculations of this type resulted in the center-section sample being common to both sets of areas. However, the area of this section was equal in the two sets of incremental areas only when the center of the sample from the center section corresponded to the center of the disk. Areas other than the center section were annular rings in both sets of incremental areas.

When the densities of samples on one side of the center of the disk were weighted according to their corresponding incremental areas and added, they gave an area mean density for the entire disk. This method of calculating the mean density was checked experimentally and was found to be satisfactory. If the area mean density based on either set of incremental areas differed by more than 10% from the average of the two sides, the results were discarded. Densities and a corresponding set of incremental areas for disks pressurized for 1 minute are presented in Table I.

Density profile curves for the disks of Table I give the variation in density across a disk that is needed to approximate experimentally the force distribution across a Type I pressure cell. Examples of these curves are shown in Figures 4 and 5. Figure 4 illustrates how well the technique developed succeeded in producing a symmetrical compression of the disks and should be compared with Figure 6, which is an example of a disk that has been prepared by metallographic

methods and pressed between anvils that had been ground external to the press. Figure 5 shows the more usual case of a density profile curve. The appearance of the curve in Figure 5 gives the idea that the compression might not have been symmetrical. However, symmetry in compression of the disks with curves such as Figure 5 was checked by the method of area mean density described in the foregoing and was found to fall within the 10% limit. The left side of Figure 5 is especially good in showing how the thrust starts at zero at the edge, increases to some maximum value, and decreases to the minimum value in the center. The distribution of force shown in Figures 4 and 5 represents experimental proof that the approximation of the second order which was first stated and then disregarded by Bridgman in calculating the average pressure for his shear experiment is of a much larger magnitude than was heretofore suspected.

THEORETICAL CONSIDERATIONS OF FORCE DISTRIBUTION OVER TYPE II PRESSURE CELL

During experimental runs to determine the best dimensions for the Type II pressure cells (see Figure 1), characteristics of these cells were repeatedly observed from which conclusions could be drawn concerning the force distribution. These characteristics included (1) flow of the pipestone ring toward the center until halted by the outward flow of the center section, (2) repeated blowouts when the pipestone ring was not thick enough to develop sufficient friction before loading the center section, and (3) extrusion of either silver chloride or lead if the amount of these solid pressure-transmitting materials were too great.

Judging by these characteristics, the mechanism for successful loading appeared to begin with the crushing of the pipestone ring, the thrust initially being supported by this ring. As the ring thickness decreased owing to the flow of the pipestone with increasing thrust, part of the thrust was transferred to the center section of the cell. Tests made in pipestone rings without any center section showed that the rings would flow until the entire flat surface of the anvil was covered. As the flow of the pipestone ring continued, a larger fraction of the total thrust was transferred to the center section and the back pressure on the ring continued to increase. The force caused by this back pressure on the pipestone ring was opposed by the frictional force between the ring and the anvil surfaces. That this frictional force at times did not become large enough

to equal the back pressure caused by the center section was assumed to be the reason for the blowouts. Results of tests made to check this assumed reason for blowouts are presented in Table II. For these tests, the thickness of the pipestone rings and the diameter of the center section were held constant, whereas the total thickness of the center section was varied. The center section with a thickness of 0.007 in. showed the characteristic extrusion of the silver chloride, whereas the 0.006-in. thick center section was completely contained. This observed extrusion characteristic indicates that when the amount of center-section material is decreased below the amount required to avoid blowout, the effectiveness of center-section loading can be gaged by the tendency to extrude from this section.

Based on the foregoing Type II pressure-cell characteristics, together with the additional supporting experimental evidence, the theoretical force distribution over the cell can be calculated by equating the frictional force between the pipestone ring and the anvil surfaces to the force exerted by the lead or silver chloride on the inside surface of the pipestone ring. Thus,

$$F_f = F_a \quad (2)$$

where the subscripts *f* and *a* refer to the frictional force and force on the inside surface of the pipestone ring, respectively. The frictional force can be expressed in terms of the coefficient of friction, *k*, and the force on the ring, F_o , as

$$F_f = 2kF_o \quad (3)$$

The force on the ring is related to the total force on the cell, F_t and the force on the center section, F_c by

$$F_o = F_t - F_c \quad (4)$$

If the solid transmitting the pressure in the center section exhibits little internal shearing stress, the pressure developed in this section is given by

$$P_c = \frac{F_c}{\pi R_1^2} \quad (5)$$

where R_1 is the radius of the center section. By using the value of pressure from equation (5) and the thickness of the pressure cell under load as *y*, the force on the inner surface of the pipestone ring can be determined from

$$F_a = \frac{2F_c y}{R_1} \quad (6)$$

Equations (2) through (6) can then be combined and arranged to give the fraction of total force over the center section as

$$\frac{F_c}{F_t} = \frac{1}{\frac{y}{kR} + 1} \quad (7)$$

Calculations made with equation (7) are based on the two assumptions that the anvil surfaces are flat under load and that the loading of the cell takes place in a definite series of steps as force is being applied. These steps include (1) an initial period when the pipestone ring receives the entire force and is crushed until the coefficient of friction reaches a maximum constant value, (2) a second period during which additional applied force is distributed between the center section of the cell and the pipestone ring, and (3) a final period in which the entire cell, with center section contained, assumes a thickness determined by a balance of the frictional and total applied force. The reliability of the first assumption has been checked for a pressure cell similar to the Type II cell used in the present investigation by Professor George Jura who used X-ray procedures [7]. The distortion of the anvils under load according to Jura's X-ray pictures is very slight. The conditions of the second assumption were observed to be at least approximately valid for all experimental runs made with the Type II cells.

Equation (7) could be used to determine the approximate pressure to which the center section of the cell has been subjected if the coefficient of friction, k , were available. Values of the coefficient of friction from independent tests under these high pressures are not available. The value, however, of k calculated by using a uniform pressure distribution and typical cell dimensions is approximately 0.025. This small value for a coefficient of friction would seem to indicate that the calculation of disk pressures for the Type II pressure cell, in which a total thrust and the anvil area are used, yields a conservative figure.

EXPERIMENTAL DETERMINATIONS OF FORCE DISTRIBUTION OVER TYPE II PRESSURE CELL

To test the validity of calculating the center-section pressure for the Type II pressure cell by the use of a uniform force distribution, as suggested by the foregoing theoretical considerations, the advantage of replacing the

radioactive sample with some pressure-sensing element at once became apparent. This pressure-sensing element had to be calibrated to pressures of more than 100,000 atm, the working pressure of the cell. The previous work with silica glass suggested the use of this material as the pressure-sensing element if a function of permanent change in density versus pressure could be determined. This function could have been determined experimentally if an apparatus were available for compressing glass disks hydrostatically above 100,000 atm. The need for this type of apparatus was eliminated by evaluating the force distribution data obtained in connection with the Type I pressure cell. The evaluation (as discussed below) of the force distribution data in Table I was accomplished in a manner such that a hydrostatic pressure could be determined whenever a uniform permanent change in density of a glass disk was obtained.

Several attempts were made to find a logical mathematical relation between the irreversible compression of glass and pressure. These attempts were based on the data of Table I. No satisfactory method was found, however, and it became necessary to use what might be termed a "relaxation" method. This method involved a type of trial-and-error procedure. The general condition used in this procedure was that the sum of the products obtained by multiplying each incremental area of a particular disk listed in Table I by the unit pressure on that area had to be equal to the total force applied on the disk. The unit pressures on the incremental areas of any disk were determined by using the corresponding values of change in density presented in Table I. In making these determinations of unit pressures, it was necessary to have the desired relation between the hydrostatic pressure and the permanent change in density.

As a starting point in the calculation procedures, the average pressure and area mean density were calculated for the disks of Table I. As shown in Figure 7, the data from this calculation were plotted and a preliminary curve was drawn. With this assumed curve available, the unit pressures on the incremental areas of each disk were determined. These values of pressure were converted to force by using the corresponding incremental areas. The calculated force on a disk was obtained by summing the forces on the incremental areas of the disk. The calculated values of force based on the preliminary curve were then compared with the measured value of force on a disk by the method shown in Table III.

A nonzero sum for the values in the fourth column of Table III was taken as proof that the preliminary curve did not give the best representation of the data. The slope and height of the preliminary curve were corrected, and the method of calculation described in the foregoing was repeated. This procedure of changing the preliminary curve and recalculating was followed until the sum mentioned in connection with the fourth column of Table III was zero. The curve used in the final calculation is shown in Figure 8.

To determine the influence of time of pressurization on the percentage change in density of silica glass, and thus determine if the function between change in density and in pressure, as given by Figure 8, would be affected, several tests were run in which different pressurization times were used at the same total thrust of 64,300 lb. The time of pressurization in these tests ranged from .1 to 128 minutes. The area mean density of each disk was calculated, the techniques described in the foregoing being used. Within the limits of experimental error, these densities remained the same, as shown in Table IV.

The function of percentage change in the density of silica glass versus the pressure as given by Figure 8 now being available, experiments were performed by replacing the radioactive sample in the lead-modified Type II pressure cell with silica glass disks which were to be used as pressure-sensing elements. The procedures used for these experiments are best illustrated by a typical example in which the anvil area had a diameter of 0.400 in. The outside diameter of the pipestone ring was the same as the anvil diameter and the inside diameter was 0.250 in. The height of the pipestone was 0.012 in. The glass disk used was 0.008 in. thick and 0.175 in. in diameter. The lead disks used to surround the glass disk had the same diameter as the inside diameter of the pipestone ring and were 0.002 in. thick. After assembly of the pressure cell, a total thrust of 113,200 lb. was applied over the cell and released. The center section of the cell was removed and cut in half. This cutting revealed a cross-sectional view of lead-glass-lead which appeared to be sufficient to eliminate any shear component in the glass. Both halves of the center section were placed in hot concentrated sulfuric acid and the lead was dissolved from around the glass. The range of the percentage change in density of the glass which was

completely fragmented was measured, the sink-float method being used, by determining the density of the fluid with all particles floating and with all particles sinking. This range of percentage change in density of the silica-glass pressure-sensing element was then converted to a pressure range by means of Figure 8.

The range of pressure for the foregoing example was between 67,000 and 77,000 atm as compared with the average pressure of 61,000 atm over the center section area of the cell. This average pressure was calculated by using the total thrust applied and the anvil surface area. The range of pressure for other tests was also higher than the calculated average pressure. The fact that the values of the pressure range determined from the silica glass pressure-sensing elements were always greater than the average pressure may be taken as experimental evidence that calculations of pressure based on a uniform force distribution over the Type II pressure cells are on the conservative side.

Mention should be made that Bridgman,[4] in attempting to obtain approximate hydrostatic pressure on glass disks, used the same type of pressure cell as described in the foregoing. He reported that no change in density was observed owing to the absence of a shearing component which was present when the force had been applied in his previous experiments with Simon [3]. Thus, he concluded that under hydrostatic pressure silica glass is not irreversibly compressed and, as a corollary, that shearing action is necessary for a permanent increase in density with pressure.

Since these results of Bridgman did not agree with those of the present investigation, a close examination of the two experimental procedures was made to try to explain the difference in the results. For Bridgman's tests, the pressure cells were of such a size that the amount of lead surrounding the glass disk was somewhat greater than in the present investigation, and the possibility exists that the glass disks in the present experiments actually experience a slight shearing component of force. Evidence of these shearing components may be found in the range of density shown by disks in the present investigation instead of a uniform density change. These ranges in density, however, were not very great when compared with the range of density shown by a glass disk pressed between two anvils. The low accuracy of the method used by Bridgman to determine changes in density of his glass

pressure-sensing elements may also account for the difference in results. The method used was merely that of measuring any change in thickness of one of the several clear blocks which had cracked from the original glass disk measuring 0.006 in. These measurements were reported accurate to within 0.0001 in., but this means that changes in density greater than 1.6% only could be observed. Another discrepancy between the two experiments was the condition of the glass disk after pressing. The complete fragmentation of the glass disk in the present investigation as compared with slight cracking only in Bridgman's test may indicate either the use of insufficient lead in the present investigation or incomplete loading in Bridgman's case. One final difference in the two experiments was that Bridgman used soda glass whereas the present tests were performed with silica glass.

TABLE I. EXPERIMENTAL DATA FOR SILICA GLASS

Disk No.	Force (lb.) x 10 ⁻⁴	Change in density (%)	Incremental areas (in. ²) x 10 ²
1	1.45	0.05	2.54
		0.1	2.42
2	2.08	0.1	Complete Disk
3	2.87	0.1	3.05
		0.5	1.74
4	3.57	0.6	2.69
		2.0	1.50
5	4.25	0.3	1.91
		2.2	3.08
6	4.28	0.3	1.21
		0.5	1.45
		2.2	1.64
7	5.66	3.6	2.04
		6.1	3.40
8	6.43	1.5	1.37
		5.2	3.42
		2.0	1.50

TABLE I (Continued)

Disk No.	Force (lb.) x 10 ⁻⁴	Change in density (%)	Incremental areas (in. ²) x 10 ²
9	8.46	2.1	0.64
		6.0	2.63
		6.1	1.72
10	8.51	1.8	0.88
		4.6	1.84
		7.7	2.04
11	9.84	5.3	0.30
		7.4	1.30
		14.9	1.69
		5.4	2.30
12	9.90	2.8	0.93
		4.0	1.10
		7.5	3.15
13	11.26	4.5	0.02
		5.1	0.62
		6.8	1.28
		12.9	1.72
		8.7	1.72
14	11.27	6.7	1.20
		8.9	3.11
15	14.06	4.0	1.72
		9.0	1.65
		8.7	1.99
16	14.09	4.3	1.54
		14.9	0.90
		7.8	1.94

TABLE II. EFFECT OF CENTER-SECTION THICKNESS ON BLOWOUT IN
SILVER CHLORIDE-MODIFIED TYPE II PRESSURE CELL

Thickness of center section (in.)	Total thrust at blowout (lb.)
0.010	15,000
0.009	26,000
0.008	47,000
0.007	200,000*
0.006	200,000*

* No blowout occurred with these disks.

TABLE III. COMPARISON OF MEASURED AND CALCULATED VALUES
OF FORCE

Disk No.	Measured force (lb.) x 10 ⁻⁴	Calculated force (lb.) x 10 ⁻⁴	Difference between calculated and measured force (lb.) x 10 ⁻⁴
1	1.45	2.16	+0.71
3	2.87	3.24	+0.37
4	3.57	4.32	+0.75
5	4.25	5.60	+1.35
6	4.28	4.44	+0.16
7	5.66	9.40	+3.74
8	6.43	9.40	+2.97
9	8.46	8.87	+0.41
10	8.51	8.30	-0.21
11	9.84	12.20	+2.36
12	9.90	9.60	-0.30
13	11.26	11.94	+0.68
14	11.27	10.70	-0.57
15	14.06	10.97	-3.09
16	14.09	9.13	-4.96

TABLE IV. INFLUENCE OF TIME OF PRESSURIZATION

Time of pressurization (minutes)	Change in area mean density (%)
1	3.6
2	3.4
8	2.8
32	3.9
128	3.5

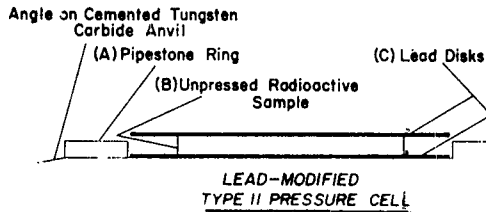
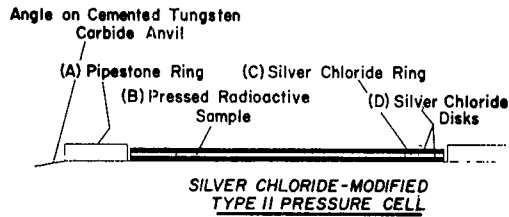
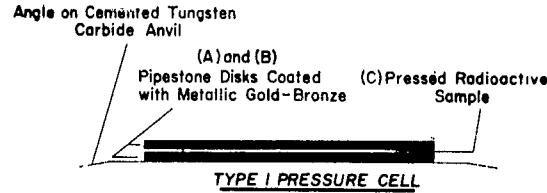


Fig. 1. Pressure cells on bottom anvil before compression.

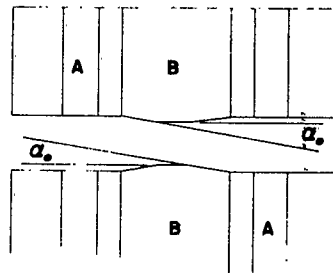


Fig. 2. Schematic diagram of anvil assembly.

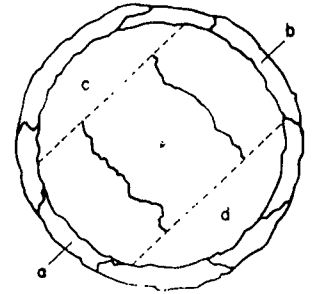


Fig. 3. Crushed glass disk showing method of sampling.

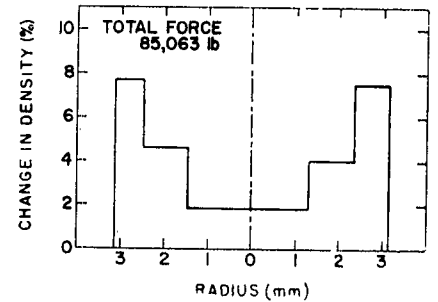


Fig. 4. Density profile of a symmetrically loaded disk, with approximately equal area samples taken 180° apart.

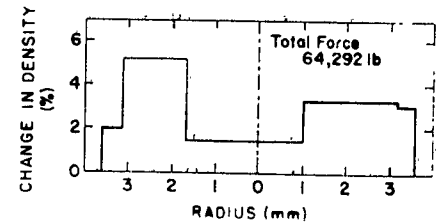


Fig. 5. Density profile of a symmetrically loaded disk, with unequal area samples taken 180° apart.

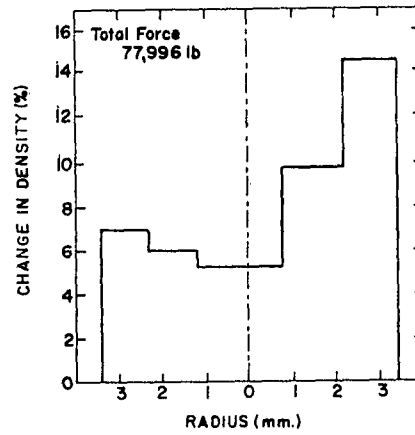


Fig. 6. Density profile of an unsymmetrically loaded disk.

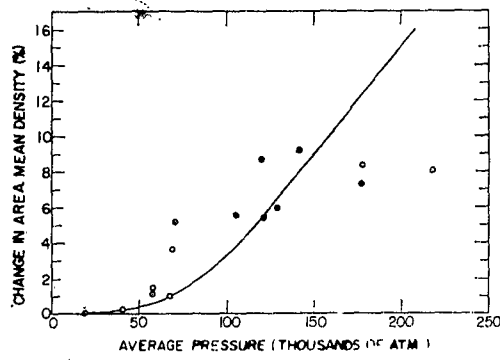


Fig. 7. Data based on area mean density and average pressure with preliminary curve used in determining the unit pressures on incremental areas.

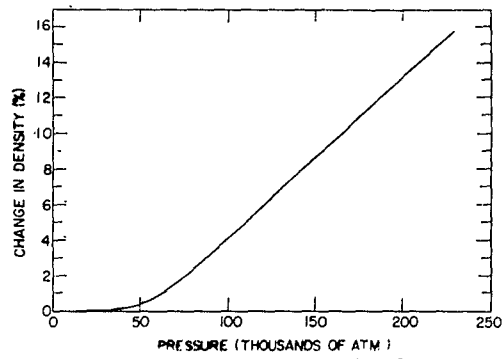


Fig. 8. Percentage change in density versus pressure for silica glass.

LITERATURE CITED

1. Bridgman, P. W., "Effects of High Shearing Stress Combined with High Hydrostatic Pressure," *Phys. Rev.*, 48, 825-47 (1935).
2. Bridgman, P. W., "Shearing Phenomena at High Pressures, Particularly in Inorganic Compounds," *Proc. Am. Acad. Arts Sci.*, 71 [7] 387-460 (1937).
3. Bridgman, P. W., and I. Simon, "Effect of Very High Pressures on Glass," *J. Appl. Phys.*, 24 [4] 405-13 (1953); *Ceram. Abstr.*, 1953, September, p. 168g.
4. Bridgman, P. W., "Miscellaneous Effects of Pressure on Miscellaneous Substances," *Proc. Am. Acad. Arts Sci.*, 84, 111-29 (1955).
5. Gogarty, W. B., S. S. Kistler, and E. B. Christiansen, "Design and Construction of Multi-Ring Apparatus for Use at High Pressures," *Rev. Sci. Instr.*, 32 [7] 775-79 (1961).
6. Gogarty, W. B., "Effect of Pressure on Orbital Electron Capture." This work formed part of a doctoral dissertation and was submitted to the Department of Chemical Engineering, University of Utah, 1960.
7. Jura, G., Department of Chemistry, University of California, Berkeley, California, personal communication.
8. Komkov, W., "A Special Case of Contact Elasticity," Office of Naval Research Tech. Report. No. IV, Contract Number NONR 1288 (02) Project Number NR-052-357, University of Utah, Salt Lake City, Utah, 1958. 40 pp.
9. Love, A. E. H., *Treatise on Mathematical Theory of Elasticity*, 4th ed. (revised), p. 192. Dover Publications, Inc., New York, 1944. 643 pp.

SECTION III

THE EFFECT OF PRESSURE ON ORBITAL ELECTRON CAPTURE

(W. B. Gogarty, S. S. Kistler, and E. B. Christiansen)

ABSTRACT

Results are presented of an experimental investigation [9] of the effect of pressure on orbital electron capture in Be^7 and Ba^{131} . Isotope samples were subjected to pressures as high as 157,000 atm for 20 days and as long as 48 days at 140,000 atm. A counting technique was employed by which small differences in the decay constants of two samples, one of which had been pressurized, were determined accurately with a scintillation system. Based on a least squares analysis of the data, the fractional increase in the total decay constant per atmosphere was estimated to be 2.5×10^{-8} and 1.3×10^{-8} for the two different cell designs in which Be^7 was pressurized and 0.66×10^{-8} for Ba^{131} which was pressurized in a third type of cell. Six out of a total of 24 runs showed a decrease in the decay constant outside of the statistical error. The reason for these six theoretically anomalous results is discussed.

INTRODUCTION

Radioactive decay by orbital electron capture is a transformation process in which the atomic number of the parent atom is reduced by one because of a proton-to-neutron conversion in the nucleus. This proton-to-neutron conversion is accomplished when an electron normally external to the nucleus, and usually one of the orbital electrons from an inner shell, is captured while inside the nucleus by a proton. By assuming the transformation process to take place only with electrons bound to the radioactive atoms, the total decay constant for the process can be written as

$$\lambda_t = C \left([\psi(0)_K]^2 + [\psi(0)_L]^2 + [\psi(0)_M]^2 + \dots \right), \quad (1)$$

where C is a constant and $\psi(0)$ represents the wave function at the nucleus for electrons from the K, L, M, etc., shells. The assumption inherent in Equation (1), which is usually justified, is that the energy required to remove an orbital electron from an electron shell such as the K shell is small compared with the total energy of the transformation. The total rate constant for decay or total decay probability of a nucleus as a result of the capture of orbital electrons is by Equation (1), proportional to the electron density within the nuclear field.

The suggestion was first made independently by Segre [15] and Daudel [7] that the rate constant for isotopes decaying by orbital electron capture might be changed by varying the electron density within the nuclear field. Several investigators [1-4, 11-13, 16, 17] have reported variations in the rate constant of Be^7 in consequence of change in the chemical environment. No results have been published on attempts to alter by physical methods the rate constants of isotopes decaying by orbital electron capture.

The decay rate for the isomeric transition in Tc^{99m} depends on the internal conversion process. In this process, some of the transition energy is removed by orbital electrons. Bainbridge [6] has observed an increase of 0.025 per cent in the decay rate of Tc^{99m} at a pressure of 100,000 atm. The results of a theoretical calculation by Porter and McMillan [14] show that the increase

in decay rate at this pressure should be in the range of 0.02 - 0.04 per cent. These experimental and theoretical results would indicate that the electron density increases at the nucleus when the average electron density of a material is increased by extremely high pressures. Since the rate constant for the electron capture process is predicted to be a function of the electron density at the nucleus, increases in the average electron density by pressure should increase the rate of radioactive decay for isotopes which normally decay by orbital electron capture.

This paper gives the method used and results obtained for an experimental study [9] undertaken to investigate the postulate that the rate of radioactive decay involving orbital electron capture may be affected by pressure-induced increases in the average electron density. The general modus operandi was to subject radioactive nuclei which normally decay by orbital electron capture to extremely high pressures and compare the rate of decay for pressurized samples with those decaying at one atmosphere.

EXPERIMENTAL

SELECTION OF RADIOACTIVE ISOTOPES

Atomic number considerations would indicate that an increase in pressure will probably change the rate of electron capture to the greatest extent in a nucleus with a smaller atomic number. However, decay by orbital electron capture is favored in elements having large atomic numbers. Thus, it is not surprising that only two isotopes (Be^7 and A^{37}) with atomic numbers less than 19 decay by electron capture. Argon is difficult to work with in a high pressure apparatus. However, Be^7 and many of its ionic salts are solids at ordinary conditions, and it has a half-life which was acceptable for use in this investigation. Therefore, Be^7 was selected as one of the isotopes to be used in the investigation. The choice of Be^7 was also influenced by the work of previous investigators who have, as noted above, succeeded by chemical means in changing its total decay constant.

The possibility exists that elements with larger atomic numbers and large factors of compressibility may experience large enough volume changes with extremely high pressures to overshadow atomic number considerations. In order to check the idea that a large compressibility may be as important as a small change in volume for barium when the pressure is increased to 100,00 kg/cm^2 from 1 kg/cm^2 has been determined by Bridgman [5] to be 45 per cent. That the isotope has a half-life of 12.0 days [18] and is readily available were also factors in its selection.

PRESSURE CELLS

Two different types of pressure cells were used to contain the radioactive samples during the application of the high pressures. The design of both of these cells was based on the physical properties of catlinite[‡]. This material exhibits a high internal shearing stress and when in contact with most metal surfaces, produces a high coefficient of friction. Cross-sectional details

[‡] The red variety of catlinite was obtained from Ward's Natural Science Establishment, Rochester, New York, under the commercial name of pipestone.

of the cells used in the investigation are presented in Figure 1.* Dimensions of the cells appear in Table I.

As the flat anvil surface on which the Type I cell rests is moved against a similar, stationary surface, the two pipestone disks are forced together and begin to flow outward in such a way as to completely contain the radioactive sample. This outward flow continues as the total thrust is increased until the internal shearing stress of the assembly equals the value of the force causing the flow. The dimensions of the disks were adjusted to limit the amount of pipestone that flowed beyond the perimeter of the flat surfaces of the anvils. A separate investigation reported in Section II and elsewhere [8, 9] revealed that the force distribution over this Type I cell is not uniform; nevertheless, all pressures for this cell are reported in terms of the total force divided by the flat-surface area of the anvil.

In the case of the Type II pressure cells (see Figure 1), the pipestone ring is initially crushed and flows both away from and toward the center section of the cell until loading of the center section begins. The force on the center section, which contains a material of low shearing stress, causes an outward force on the pipestone ring which is balanced by the frictional force on the ring. Observations [8, 9] (see Section II) have shown that the pressures developed on samples within the center sections of these cells are approximately uniform and can be calculated by dividing the total thrust by the anvil area. Pressures reported for the Type II cells were calculated in this manner.

PRESSURE EQUIPMENT

Total thrusts for the above described pressure cells were furnished by one 50-ton press and two 100-ton presses. The 50-ton press was manufactured by American Steel Foundries (Elmes Engineering Division). The 100-ton presses were designed and constructed for the investigation [9]. All presses were fitted with pressure-recording and control units by which the cylinder oil pressure was recorded and kept constant during a run. Presses were equipped so that the rate of increasing and decreasing the thrust could be varied. The adjustment of the rate of application or removal of thrust was necessary

*Figures for Section III are found on pp. 57-64.

in some cases to avoid cell failure by "blowout". The total thrust on the pressure cells was taken as the total force applied to the piston of the press used. This method of determining thrust on the cells assumes that loss of force caused by friction in the press packing glands is negligible. This assumption was checked for the presses by use of a calibrated load cell, and the effect of packing gland friction was found to be negligible.

Thrust was transmitted from a particular press to one of the pressure cells by means of the anvil assembly shown in cross section in Figure 2. The central portions of this assembly, listed as B in Figure 2, will be referred to as the anvils. Identical truncated conical tops having the required angle, α_0 , and dimensions to give the desired strength and flat working surface were ground on each of these anvils. Anvils were made of cemented tungsten carbide. The shrunk-on steel rings, listed as A in Figure 2, were designed and fabricated to furnish the required external support to the anvils [9, 10]. (See Section I).

RADIOACTIVE COUNTING

Changes in the total decay constant of isotopes subjected to pressure were measured by a comparison type of counting technique. This technique eliminated the need for determining an accurate-absolute value of isotope half-life and also minimized the influence of electronic drift in the equipment. The technique used was based on the following relationship

$$\frac{\left(\frac{dA}{dt}\right)_{p_t}}{\left(\frac{dA}{dt}\right)_{s_t}} = \frac{\left(\frac{dA}{dt}\right)_{p_o}}{\left(\frac{dA}{dt}\right)_{s_o}} \exp\left[-\left(\lambda_p(t_{p_t} - t_{p_o}) - \lambda_s(t_{s_t} - t_{s_o})\right)\right], \quad (2)$$

where dA/dt represents an average value of the measured activity, λ is the total decay constant, and t is the time. The subscripts p , s , o , and t in the above equation refer to the pressurized sample, the standard sample, an initial time, and any time, respectively.

Equation (2) is based on the fundamental relationship giving the rate

of decay of N radioactive atoms as

$$\frac{dN}{dt} = -\lambda_t N . \quad (3)$$

In deriving Equation (2), Equation (3) is first integrated between an initial time, t_o , and any time, t , and then multiplied by λ_t to give

$$\left(\frac{dN}{dt}\right)_t = \left(\frac{dN}{dt}\right)_o \exp\left[-\lambda_t(t - t_o)\right] . \quad (4)$$

The absolute activity in Equation (4) is next replaced with the measured activity by means of Equation (5)

$$\frac{dN}{dt} = K \frac{dM}{dt} , \quad (5)$$

which results in Equation (6)

$$\left(\frac{dM}{dt}\right)_o = \left(\frac{dM}{dt}\right)_t \exp\left[-\lambda_t(t - t_o)\right] . \quad (6)$$

The activities in Equation (6) are the instantaneous or point values at an initial time, t_o , and some later time, t . The average activity, measured over a time interval, θ , can be related to the instantaneous activity at time t_o by

$$\left(\frac{dA}{dt}\right)_o = \frac{1}{\theta} \left(\frac{dM}{dt}\right)_o \int_{t_o}^{t_o + \theta} \exp\left[-\lambda_t(t - t_o)\right] dt . \quad (7)$$

The integrated and rearranged form of Equation (7) is

$$\left(\frac{dM}{dt}\right)_o = \frac{1}{\theta} \left(\frac{dA}{dt}\right)_o \frac{\lambda_t \theta}{1 - \exp[-\lambda_t \theta]} \quad (8a)$$

The integration of Equation (7) over the same time interval, θ , but with limits fixed by a later time, t , results in

$$\left(\frac{dM}{dt}\right)_t = \left(\frac{dA}{dt}\right)_t \frac{\lambda_t \theta}{1 - \exp[-\lambda_t \theta]} \quad (8b)$$

The instantaneous values in Equation (6) can then be replaced by using Equations (8a) and (8b) to give

$$\left(\frac{dA}{dt}\right)_t = \left(\frac{dA}{dt}\right)_o \exp. \left[-\lambda_t (t - t_o) \right] \quad (9)$$

The division of Equation (9) for a pressurized sample by the same equation for a standard sample completes the derivation of Equation (2).

During the time preceding or following the application of pressure to the pressurized sample, the value of the rate constants in Equation (2) will be equal so that

$$\frac{\left(\frac{dA}{dt}\right)_{p_t}}{\left(\frac{dA}{dt}\right)_{s_t}} = \frac{\left(\frac{dA}{dt}\right)_{p_o}}{\left(\frac{dA}{dt}\right)_{s_o}} \exp. \left[-\lambda_s (\Delta t_o - \Delta t_t) \right], \quad (10)$$

where Δt_o and Δt_t represent the quantities $\left(t_{s_o} - t_{p_o} \right)$ and $\left(t_{s_t} - t_{p_t} \right)$, respectively.

Equation (10) shows that if the difference in counting-starting time, Δt_t , is always kept equal to the initial starting time difference, Δt_o , the measured ratio of the activity of the two samples will remain constant. Repeated counting of the standard and then the pressurized sample in accordance with Equation (10) permits the determination of the ratio of activity of the samples before and after pressurization. This cyclic type of counting for

short-time intervals is one of the means of minimizing the effects of electronic drift.

The fractional change in the decay constant can be calculated by applications of Equation (2) to the period of pressurization. For this period of time, Equation (2) becomes

$$\frac{\Delta\lambda}{\lambda_s} = \frac{1}{\lambda_s t} \left[1 - \frac{r_f}{r_i} \right]. \quad (11)$$

Equation (11) is obtained by first using r_i and r_f for the initial and final ratios of sample activity in Equation (2) and then taking t_{p_0} and t_{s_0} equal to zero, with t_p and t_s equal to the time of pressurization, t . Next, the exponential is expanded and second order and higher terms are disregarded because $\Delta\lambda$ is small. Both sides of the expression are then divided by λ_s , and the final rearrangement made.

Isotope activities used in the above equations were determined experimentally by counting the gamma rays emitted from an excited-energy level of the decay product. The 477 kev excited level of Li^7 was used for Be^7 , and the 494 kev excited level of Cs^{131} was used for Ba^{131} . These rays were counted with a single-channel differential-scintillation spectrometer. The instrument used was manufactured by Baird-Atomic, Inc., of Cambridge, Massachusetts and is commercially available as Model 516.

The maximum number of counts per unit time associated with the photoelectric peaks of the above energy levels were determined during each run. This was accomplished by first adjusting the amplifier so that the voltage difference between position of minimum counting on each side of the photopeak was equal to seven volts, the maximum separation voltage between the lower and upper discriminator for the instrument used. Lower and upper discriminators were then made to correspond with the minimum counting values preceding and following the photoelectric peak. In addition to obtaining the maximum number of counts by adjusting the discriminators in the above manner, the effects on counting accuracy caused by electronic drift in the equipment were appreciably reduced.

Any error in the change of the total decay constant as calculated from Equation (11) depends on the accuracy with which r_f/r_i is determined. The two sources of error inherent in radioactive counting associated with this ratio are statistical fluctuations and effect of background activity. These sources of error were taken into account in the above counting technique by the methods described in the following paragraphs.

If all units of the spectrometer are operating properly so that only random radioactive disintegration events are being recorded in the scaler, the counting standard deviation for either a pressurized or standard sample is

$$\Delta = (\sum_i A_i)^{\frac{1}{2}} \quad (12)$$

The summation term in Equation (12) represents the addition of all counts made on a sample during the cyclic type of counting mentioned earlier. With equal counting times for the pressurized and standard sample before and after pressurization, r_f/r_i becomes

$$\frac{P_f/S_f}{P_i/S_i} \quad (13)$$

where P and S represent the total number of counts for the pressurized and standard samples, respectively. Each of the values in Equation (13) will be accompanied by a statistical error of the type shown by Equation (12). With these statistical errors included, Equation (13) becomes

$$\frac{(P_f \pm \sqrt{P_f}) (S_i \pm \sqrt{S_i})}{(P_i \pm \sqrt{P_i}) (S_f \pm \sqrt{S_f})} \quad (14)$$

Combination of the individual standard deviations in Equation (14) results in

$$\frac{P_f/S_f}{P_i/S_i} \left[1 + \sqrt{\frac{1}{P_f} + \frac{1}{P_i} + \frac{1}{S_f} + \frac{1}{S_i}} \right] \quad (15)$$

which can be used to calculate the statistical error associated with the ratio r_f/r_i .

In actual practice, a certain amount of radiation from sources other than the sample, e.g., cosmic radiation, is always counted simultaneously with the sample. The ratios used in Equation (11) must therefore be determined by means of

$$\frac{\left(\frac{d\bar{A}}{dt}\right)_P - \left(\frac{dB}{dt}\right)_P}{\left(\frac{d\bar{A}}{dt}\right)_S - \left(\frac{dB}{dt}\right)_S} = r, \quad (16)$$

where the $d\bar{A}/dt$ terms represent the average sample-plus-background activity as measured over a given time interval and the average background activity over the same time interval is given by dB/dt . With the counting equipment used, the background activity could not be determined simultaneously with the sample-plus-background activity so the effect of background was considered as described below.

Background activities were determined at various times throughout the investigation. These activities were within the ranges of 100 - 200 and 300 - 400 counts per minute for the Be^7 and Ba^{131} , respectively. However, variations in the background activity were observed to be negligible during periods of time equal to one cycle in the counting of the pressurized and standard samples. Thus, the dB/dt terms in Equation (16) could be equated, and the equation rearranged to give

$$\frac{\left(\frac{d\bar{A}}{dt}\right)_P}{\left(\frac{d\bar{A}}{dt}\right)_S} = r + \frac{\left(\frac{dB}{dt}\right)}{\left(\frac{d\bar{A}}{dt}\right)_S} (1 - r). \quad (17)$$

Equation (17) shows that with a value of r sufficiently close to 1.0000 and the sample activity much greater than background activity, the ratio r can be approximated by

$$\left(\frac{d\bar{A}}{dt}\right)_p \bigg/ \left(\frac{d\bar{A}}{dt}\right)_s$$

The use of this approximation for the investigation was checked by calculating the maximum value of the error introduced by using ratios without excluding the background activity. These calculations were made by using the maximum background activity observed during the investigation. Results of these calculations showed that for the case of Be^7 , the effect of excluding the background activity was insignificant. Thus, ratios used for calculating the fractional change in the decay constant for this isotope were determined by using the total counts obtained for a sample with the spectrometer. For the case of Ba^{131} , the effect of excluding the maximum background activity was found to be significant. Ratios for this isotope were therefore calculated by subtracting the maximum number of background counts from the total sample counts obtained in the spectrometer. The maximum number of background counts were determined by using the rate 400 counts per minute, this being the maximum value of background activity observed throughout the investigation.

SAMPLE PREPARATION

Isotopes were procured as chlorides in hydrochloric acid solution with initial activities of 0.5 millicuries ^{##}. The original solutions were first diluted, and aliquot portions were then taken which gave a measured sample activity of between approximately one-half and one-million counts per five minutes. Carrier material in the form of BeCl_2 for the Be^7 and BaCl_2 for the Ba^{131} was added to the solutions so that precipitation of samples could be accomplished by methods of ordinary quantitative analysis. Beryllium and barium samples were precipitated as the basic carbonate and sulfate, respectively. Samples were filtered by use of a suction filtering apparatus designed to give easy access to the collected disk of radioactive material.

^{##} Radioactive samples were prepared with Be^7 supplied by the Nuclear Science and Engineering Corporation of Pittsburgh, Pennsylvania, and Ba^{131} supplied by the Oak Ridge National Laboratory at Oak Ridge, Tennessee.

These disks were then used in one of the three types of pressure cells shown in Figure 1. In assembling the lead-modified Type II cells, the disks containing the radioactive material were utilized as they came from the suction filter. In the case of the Type I and silver chloride-modified Type II cells, disks from the filter were compressed before assembling in order to decrease the initial volume.

The Type I and lead-modified Type II cells were attached to the lower anvil by glue. These cells were subjected to full pressure for one day to establish the initial counting geometry with respect to the lower portion of the anvil assembly. Because of the complete containment of the radioactive sample within the silver chloride of the silver chloride-modified Type II cell, the inner portion of this cell was not attached permanently to a lower anvil. This non-attachment made the inner portion of the cell independent of a particular lower anvil and pipestone washer. The initial counting geometry for the inner portion of this cell was fixed by holding the entire cell at full pressure for one day.

COUNTING GEOMETRY

Since the Type I and lead-modified Type II cells were both attached permanently to a given lower anvil, an apparatus was needed to establish the geometry of the counting crystal with respect to the anvil. This apparatus was designed so that the crystal could be repeatedly moved between the pressurized and standard samples during the cyclic-type counting described above. In addition, the apparatus was designed to make the lower portion of the anvil assembly containing the pressurized sample capable of being moved between the counting position and press without disturbing the geometry.

Unlike the two other types of cells, the silver chloride-modified Type II cell was not attached to a particular lower anvil. The inner portions of this type of cell were therefore placed in specially designed holders [9] to establish their counting geometry. Results obtained for a counting test performed to check the reproducibility of the counting system are presented in Table II.

RESULTS

The experimental data and results of the investigation are presented in tabular form in Tables III, IV, and V. Consecutive runs obtained with the same pressurized sample are indicated in the "Number of Run" column by means of the same number followed by either the letter A or B. Dates listed in the tables include both the time for pressurization and counting. Counts reported under the various headings represent the sum of all counts taken by the comparison-counting technique described above. Values appearing under the heading entitled "Fractional Increase in the Total Decay Constant" were calculated by using the half-life of Be^7 and Ba^{131} as 53.0 days and 12.0 days, respectively [18]. For the case of Ba^{131} , values of final to initial-activity ratio were corrected as discussed above for the maximum error introduced by not excluding background activity before the calculation was made.

Results from Tables III, IV, and V are presented graphically in Figures 3 - 8. Values from the column of the corresponding table entitled either "Standard Deviation of Final Ratio/Initial Ratio" or "Standard Deviation of the Fractional Increase in the Total Decay Constant" are indicated in these figures by means of the line extending the correct graphical distance above and below each point. To the left of each point is found the number of the run.

In figures 3, 4 and 5, the values of either the pressure or average force per anvil area (average pressure) in units of 1000 atm are at the right of the vertical data spread lines. The straight but non-zero slope lines on Figures 6, 7, and 8 represent a least-squares fit of the plotted points where the intercept is zero.

DISCUSSION

At a specific pressure, Equation (11) gives a linear relationship between the quotient of the final to the initial counting ratio and time. Results of the investigation presented in Figures 3, 4 and 5, should, therefore, follow this relationship. Runs 1 through 3 of Figure 3 show the expected decrease in r_f/r_i as time increases. Run 4 of this figure also agrees with the predicted trend since $\Delta\lambda/\lambda_s$ for this run would be less because of the lower pressure. However, some of the remaining runs of Figure 3, such

as Run 5, which should be identical with Run 3, and Runs 6, 8, 10, and 11 with values for the ratio greater than 1.0000, which are not in agreement with theory, show individual disagreement with Equation (11). Similarly, results in Figures 4 and 5 are in partial agreement only with Equation (11).

Because of the scattered data in these figures, two methods were used for evaluating the results of this investigation. In the first method, individual runs were evaluated in terms of the experimental techniques used in the investigation. These techniques were considered in view of experimental difficulties which could cause the results to fall either above or below the line of no effect. The second method of evaluation averaged the results of all individual runs from a particular type of pressure cell. The evaluation of the results by these two methods is described in the following paragraphs.

The experimental difficulties considered in the first method of evaluating the results were:

1. Loss of radioactive sample from the pressurized cell;
2. Changes in the operation of the electronic counting equipment;
3. Changes in the counting geometry of the pressurized cell.

Whether the last two of these difficulties could cause errors so large that individual runs fell above or below the line of no effect is not obvious, but the first one would only cause an error such that runs fell below the line of no effect.

In checking for loss of sample, each cell was observed under the microscope to see if any breakage had occurred, and the upper anvil was counted with the idea that any sample lost from the cell would adhere to the flat surface of the anvil because of the high pressures being used. In addition, pressurized samples were repressurized when possible so that small losses would be stabilized. Runs 3A and 3B of Figure 4 are examples of this repressurizing method. The fact that the second of these runs, as well as the first, is below the line of no effect would indicate that no loss of radioactive sample occurred during the two runs.

Counting checks of the electronic equipment were made at various times throughout the investigation. The day-to-day results of these checks were always reproducible within the limits of the statistical error. The results of these checks were taken as proof that no errors were introduced by the counting equipment.

If the first two experimental difficulties mentioned above did not occur, then the last one -- changes in the counting geometry -- must have been responsible for the unexpected data in Figures 3 through 5 which appear above the line of no effect. In order to determine if a change in counting geometry because of a slight spreading of the cell increased the counting rate, an independent counting experiment was performed in which the counting rate was measured both before and after the pressure cell had been pressurized. By measuring the counting rate both preceding and following the initial pressurization of the cell when the greatest change in cell geometry occurred, the maximum effect of the spreading of the cell was probably observed. Results of this experiment are presented in Table VI. The grand average in Table VI after pressurization divided by the value before pressurization gives a quantity of 1.0097. This value represents the same type of ratio plotted in Figures 3 through 5 except that the pressurized sample was under pressure for essentially zero time and the change from 1.0000 was due to the spreading of the cell.

By examining the data for the A and B runs in Figures 3 through 5, additional evidence is found for the thesis that spreading of the pressurized cells resulted in an effect opposite to the one caused by pressure. Results for the B runs were obtained, as mentioned above, by repressurization of cells used in the corresponding A runs. Because of the additional time under pressure, the numerical values of the B runs should have been less than those of the corresponding A runs. As can be seen, the numerical results of the B runs were always greater than those of the corresponding A runs. Apparently, repressurization of the cells for the B runs caused a slight spreading of the cells with an accompanying change in counting geometry. The increased numerical values for the B runs indicate that these changes in counting geometry resulted in an effect opposite to the one caused by pressure. In fact for some of the B runs, the effects resulting from pressure were completely overriden by changes in counting geometry.

The averaging technique used in the second method of evaluating the results of this investigation was based on the fact that the value of the fractional increase in the total decay constant, $\Delta\lambda/\lambda_s$, is some function of pressure. This functional relationship formed the basis for Figures 6 through 8. It is probable that the actual changes in $\Delta\lambda/\lambda_s$ with pressure are small until pressures much higher than the ones used in this investigation are applied. For small changes in $\Delta\lambda/\lambda_s$, the relationship between $\Delta\lambda/\lambda_s$ and pressure can be approximated by a linear function. With the assumption of a linear relationship, all of the individual runs for a particular pressure cell can be averaged by means of a least-squares fit of the data. The non-zero slope lines shown in Figures 6 through 8 represent the results of averaging the data with this least-squares technique. The slopes of these lines give an indication of the fractional increase in the total decay constant per atmosphere. Values of these slopes are 2.5×10^{-8} (without Run 5), 1.3×10^{-8} , and 0.66×10^{-8} for Figures 6, 7, and 8, respectively. Both negative and positive values of $\Delta\lambda/\lambda_s$ were included in the least-squares technique so that values of the increase in total decay constant with pressure are probably on the conservative side.

CONCLUSIONS

The results of the investigation seem to justify the conclusion that pressures of a sufficient magnitude were used to increase the electron density at the nucleus so that the normal decay rates of the two isotopes used were increased. This conclusion is based on the premise that the experimental difficulties, described in the above section, are the only ones involved and that these difficulties cause values to change in the direction indicated. The conclusion that an increase in the decay rate occurred in the case of Be^7 seems especially justified since two different types of pressure cells gave a relatively large number of runs all of which showed an increase. In the case of these two different types of cells, it seems highly improbable that a repeated loss of sample could have accounted for an increase in the decay rate in all the samples that showed this increase. Although the basis for the conclusion that there was an increase in the case of Ba^{131} was made

on a much smaller number of runs than for Be^7 , the results of the runs still seem to indicate that an increase in rate of decay had been achieved.

In addition to the many individual runs which showed an increase in decay rate outside the statistical counting error, the averaged linear relationships for the two isotopes between this increase and pressure furnish further support to this conclusion. It should also be noted in connection with the values of fractional increase of the total decay constant, as caused by pressure and given by these averaged-linear relationships, that these slight increases are of the same order of magnitude as those caused by chemical combination.

TABLE I
CELL DIMENSIONS
Type I Pressure Cell

<u>Part</u>		Outside Diameter (Inches)	Thickness (Inches)
A	(Pipestone)	0.200	0.005
B		0.200	0.005
A	(Metal)	0.200	0.001
B		0.200	0.001
C		0.150	0.004

Silver Chloride-Modified
Type II Pressure Cell

<u>Part</u>	Outside Diameter (Inches)	Inside Diameter (Inches)	Thickness (Inches)
A	0.325	0.225	0.010
B	0.158		0.004
C	0.220	0.158	0.004
D	0.220		0.002

Lead-Modified
Type II Pressure Cell

<u>Part</u>	Outside Diameter (Inches)	Inside Diameter (Inches)	Thickness (Inches)
A	0.325	0.225	0.010
B	0.156		0.012
C	0.220		0.0015

TABLE II

SUMMARY OF DATA FROM TEST ON
OPERATION OF THE COUNTING EQUIPMENT

<u>Day</u>	<u>Average Ratio for Fifty Minutes</u>					<u>Grand Average for Day</u>
	<u>Run 1</u>	<u>Run 2</u>	<u>Run 3</u>	<u>Run 4</u>	<u>Run 5</u>	
0	1.3011	1.3003	1.2988	1.2982		1.2996
2	1.2981	1.3001	1.3013	1.3025	1.2992	1.3002
4	1.2997	1.2994	1.3011	1.2994	1.2999	1.2999
6	1.2983	1.3020	1.2991	1.3021	1.2990	1.3001

Table III

Data and results for Be^7 in the lead-modified Type II pressure cell

No. of Run	Dates of Run	Time Under Pressure (days)	Pressurized Sample Initial (Total Counts)	Standard Sample Initial (Total Counts)	Initial Ratio	Pressurized Sample Final (Total Counts)	Standard Sample Final (Total Counts)	Final Ratio	Final Ratio/Initial Ratio	Standard Deviation of Final Ratio/Initial Ratio	Maximum Correction to Final Ratio/Initial Ratio Excluding Background Activity	Pressure atm $\times 10^{-3}$	Fractional Increase in the Total Decay Constant	Standard Deviation of the Fractional Increase in the Total Decay Constant
1	Sept 4 Sept 10	3.83	44,496,694	27,513,098	1.6173	41,700,902	25,792,577	1.6168	0.9997	± 0.0004	0.0000	98.5	6×10^{-3}	$\pm 8 \times 10^{-3}$
2	Sept 11 Sept 22	6.78	35,740,778	22,519,449	1.5871	31,962,946	20,215,136	1.5811	0.9962	± 0.0004	+ 0.0001	99.3	43×10^{-3}	$\pm 5 \times 10^{-3}$
3	Sept 23 Oct 2	5.43	21,972,661	17,429,335	1.2507	19,955,555	15,555,217	1.2550	0.9979	± 0.0005	0.0000	100.1	39×10^{-3}	$\pm 7 \times 10^{-3}$
4	Nov 15 Nov 24	8.34	18,334,536	12,104,563	1.5146	11,460,921	7,575,279	1.5125	0.9955	± 0.0006	+ 0.0001	80.0	10×10^{-3}	$\pm 5 \times 10^{-3}$
5	Nov 22 Nov 28	5.71	8,298,645	11,329,920	0.7324	8,682,637	11,915,226	0.7270	0.9926	± 0.0006	- 0.0001	100.0	99×10^{-3}	$\pm 8 \times 10^{-3}$
6	Nov 29 Dec 10	8.92	16,203,065	12,483,182	1.2950	9,979,816	7,665,762	1.3007	1.0021	± 0.0006	+ 0.0001	96.7	$- 13 \times 10^{-3}$	$\pm 5 \times 10^{-3}$
7	Nov 29 Dec 10	6.75	7,905,378	12,212,233	0.6473	5,876,433	9,083,947	0.6469	0.9994	± 0.0007	- 0.0002	92.3	7×10^{-3}	$\pm 8 \times 10^{-3}$
8	Dec 1 Dec 8	7.53	12,582,930	10,130,759	1.2421	9,083,750	7,308,017	1.2430	1.0007	± 0.0007	+ 0.0001	119.4	$- 7 \times 10^{-3}$	$\pm 7 \times 10^{-3}$
9A	Dec 11 Dec 22	10.42	8,904,416	10,695,288	0.8326	6,417,359	7,727,601	0.8304	0.9974	± 0.0007	0.0000	95.6	19×10^{-3}	$\pm 5 \times 10^{-3}$
9B	Dec 22 Jan 7	16.08	6,417,359	7,727,601	0.8304	1,282,756	1,544,563	0.8305	1.0001	± 0.0013	0.0000	95.6	$- 0.5 \times 10^{-3}$	$\pm 6 \times 10^{-3}$
10	Dec 12 Dec 20	6.79	13,145,460	11,396,767	1.1534	12,001,532	10,393,066	1.1548	1.0012	± 0.0006	0.0000	119.4	$- 14 \times 10^{-3}$	$\pm 7 \times 10^{-3}$
11	Dec 12 Dec 22	7.89	10,504,242	11,423,833	0.9195	11,323,726	12,273,154	0.9226	1.0034	± 0.0006	0.0000	112.9	$- 33 \times 10^{-3}$	$\pm 6 \times 10^{-3}$
12	Dec 23 Jan 12	18.96	12,113,944	9,824,326	1.2331	9,415,949	7,640,369	1.2325	0.9995	± 0.0006	+ 0.0002	105.3	2×10^{-3}	$\pm 2 \times 10^{-3}$
13	Dec 24 Jan 3	9.96	9,861,643	7,821,893	1.2608	8,652,955	6,571,167	1.2608	1.0000	± 0.0007	+ 0.0001	119.4	0.3×10^{-3}	$\pm 6 \times 10^{-3}$

Table IV

Data and results for Be⁷ in the Type I pressure cell

No. of Run	Dates of Run	Time Under Pressure (days)	Pressurized Sample Initial (Total Counts)	Standard Sample Initial (Total Counts)	Pressurized Sample Final (Total Counts)	Standard Sample Final (Total Counts)	Final Ratio/Initial Ratio	Standard Deviation of Final Ratio/Initial Ratio	Maximum Correction to Final Ratio/Initial Ratio Excluding Background Activity	Average Force per Area atm x 10 ⁻³	Fractional Increase in the Total Decay Constant	Standard Deviation of the Fractional Increase in the Total Decay Constant
1	Jan 5 Jan 24	15.89	17,894,645	20,133,014	14,314,026	16,101,391	0.8886	± 0.0005	- 0.0001	112.5	2 x 10 ⁻³	± 3 x 10 ⁻³
2	Jan 10 Feb 13	33.79	19,897,483	19,224,477	7,713,620	7,459,815	1.0350	± 0.0006	+ 0.0001	80.1	2.3 x 10 ⁻³	± 1 x 10 ⁻³
3A	Jan 14 Feb 6	21.94	8,573,582	7,454,160	6,294,535	5,496,417	1.1502	± 0.0008	+ 0.0001	123.7	15 x 10 ⁻³	± 3 x 10 ⁻³
3B	Feb 6 Feb 27	20.04	6,294,536	5,496,417	4,828,107	4,223,223	1.1432	± 0.0009	+ 0.0002	123.7	6.5 x 10 ⁻³	± 3 x 10 ⁻³
4A	Jan 26 Feb 20	24.75	21,654,766	15,668,347	15,261,208	11,362,091	1.3432	± 0.0005	+ 0.0002	139.5	3 x 10 ⁻³	± 2 x 10 ⁻³
4B	Feb 20 Mar 15	23.67	15,261,208	11,362,091	3,123,851	2,322,565	1.3450	± 0.0015	+ 0.0001	139.5	4.2 x 10 ⁻³	± 3.3 x 10 ⁻³
5	Feb 15 Mar 9	20.50	3,130,744	8,225,110	3,697,035	3,746,302	0.9552	± 0.0009	0.0000	157.0	6.0 x 10 ⁻³	± 3 x 10 ⁻³

Table V

Data and results for Ba¹³¹ in the silver chloride modified Type II pressure cell

No. of Run	Dates of Run	Time Under Pressure (days)	Pressurized Sample Initial (Total Counts)	Standard Sample Initial (Total Counts)	Pressurized Sample Final (Total Counts)	Standard Sample Final (Total Counts)	Final Ratio/Initial Ratio	Standard Deviation of Final Ratio/Initial Ratio	Maximum Correction to Final Ratio/Initial Ratio Excluding Background Activity	Pressure atm x 10 ⁻³	Fractional Increase in the Total Decay Constant	Standard Deviation of the Fractional Increase in the Total Decay Constant
1	Mar 21 Mar 30	8.71	19,863,507	15,459,570	7,098,900	5,518,365	1.2849	± 0.0007	+ 0.0005	156.6	3.4 x 10 ⁻³	± 1 x 10 ⁻³
2A	Apr 23 Apr 29	5.43	41,913,095	30,553,280	18,854,531	13,784,394	1.3578	± 0.0004	+ 0.0001	156.6	8.0 x 10 ⁻³	± 1 x 10 ⁻³
2B	Apr 30 May 5	5.72	18,854,531	13,784,394	7,891,155	5,768,904	1.3678	± 0.0007	+ 0.0004	156.6	1.5 x 10 ⁻³	± 2 x 10 ⁻³

TABLE VI.

EFFECT ON THE COUNTING RATIO BY SPREADING A PRESSURE CELL

<u>Run</u>	<u>Counting Ratio Before Pressurization (50 min. average ratio)</u>	<u>Counting Ratio After Pressurization (50 min. average ratio)</u>
1	1.1599	1.1719
2	1.1603	1.1707
3	1.1624	1.1706
4	1.1611	1.1742
5		1.1736
(Grand average)	(1.1609)	(1.1722)

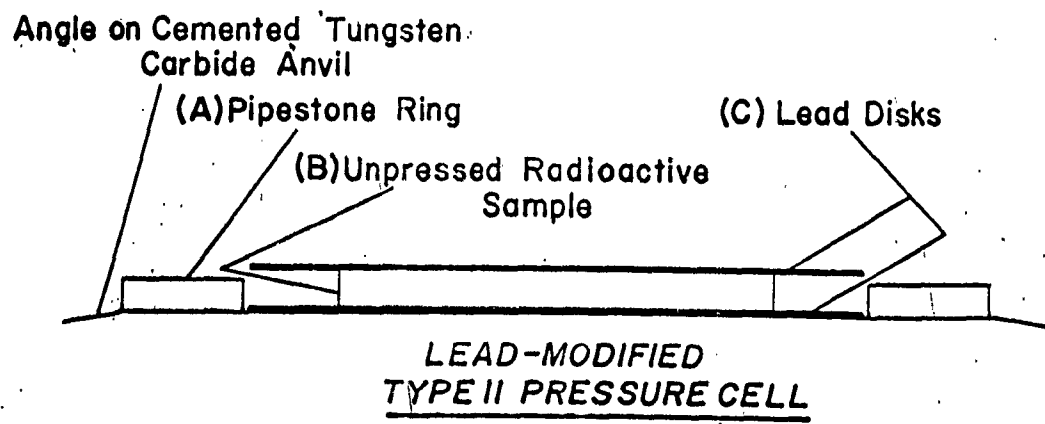
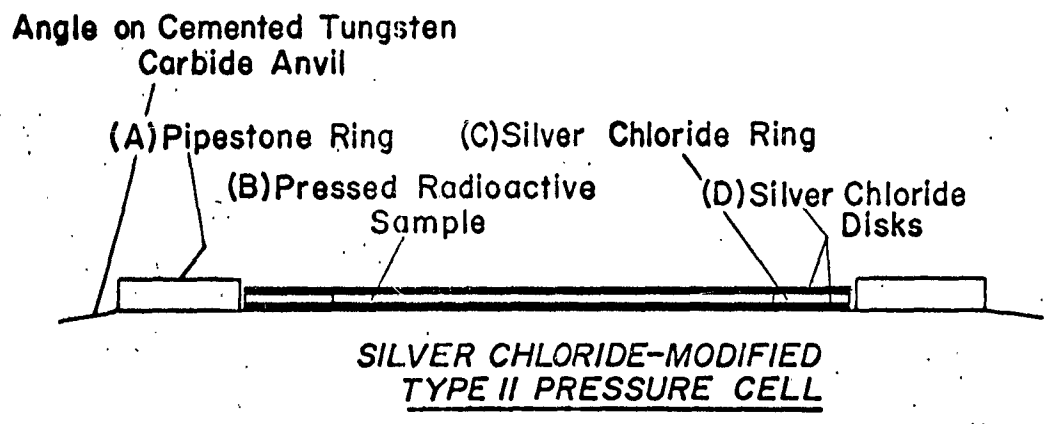
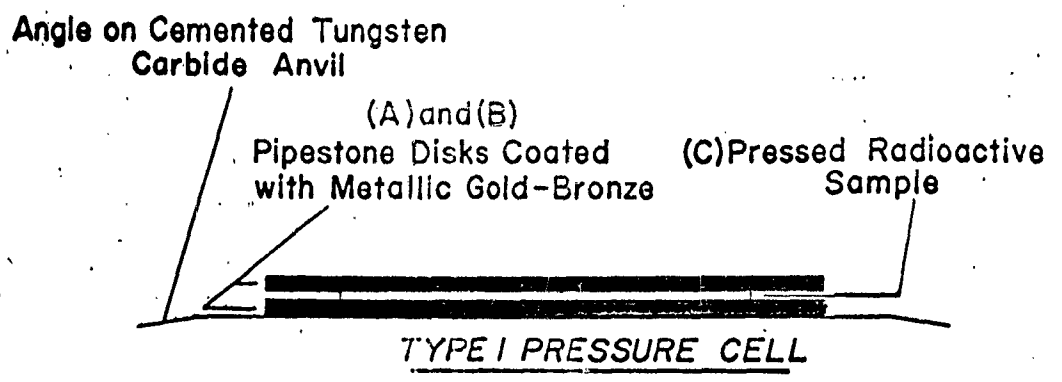


Fig. 1. Cross-sectional details of pressure cells before force has been applied.

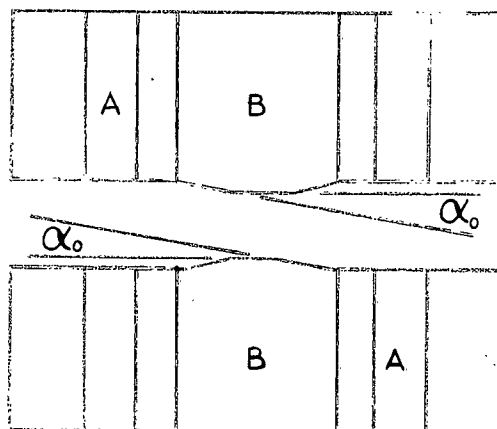


Fig. 2. Schematic diagram of the anvil assembly.

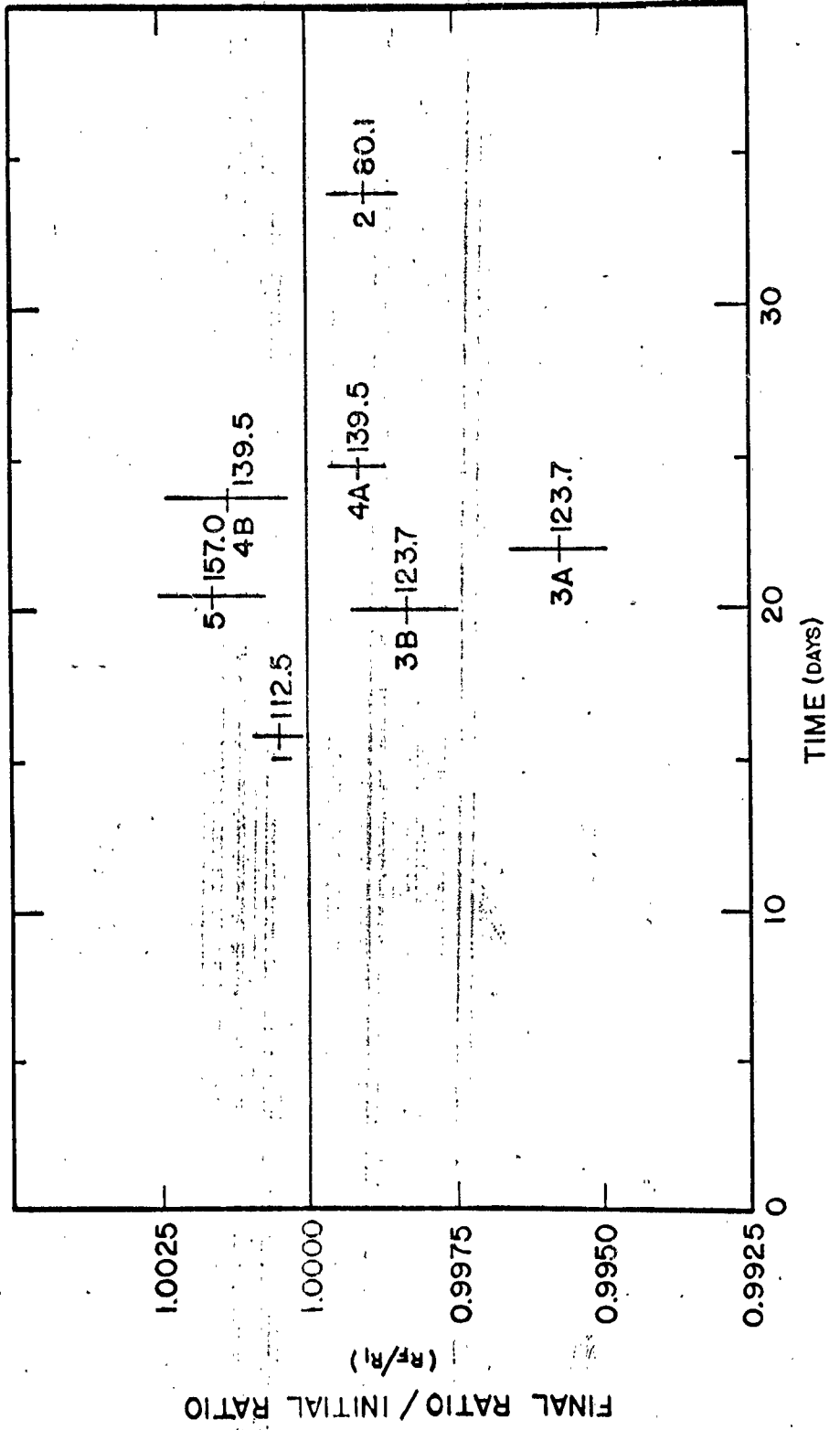


Fig. 4. Change in the final ratio/initial ratio with time for Beryllium (7) in the Type I pressure cell.

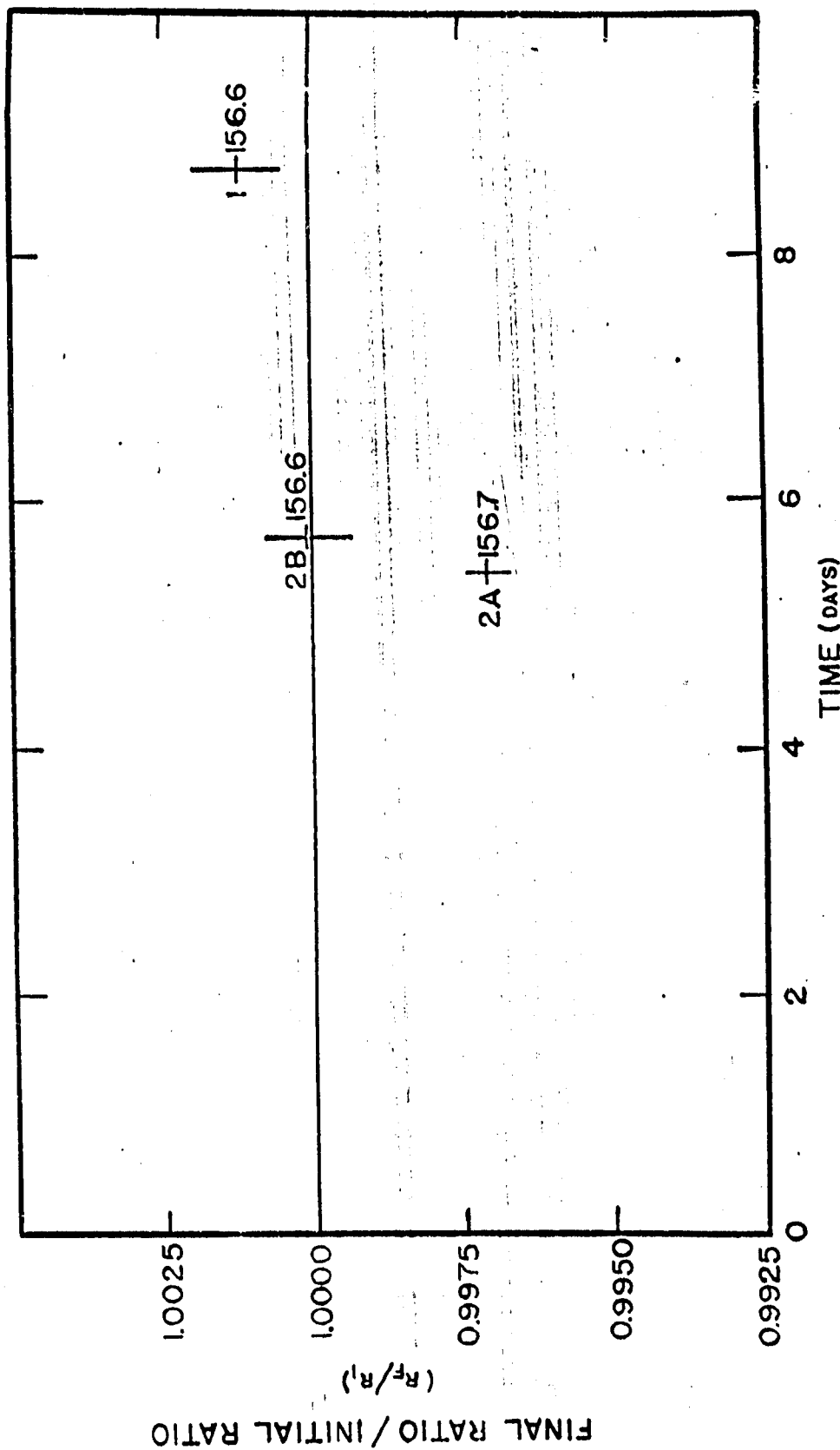


Fig. 5. Change in the final ratio/initial ratio with time for Barium (131) in the silver chloride-modified Type II pressure cell.

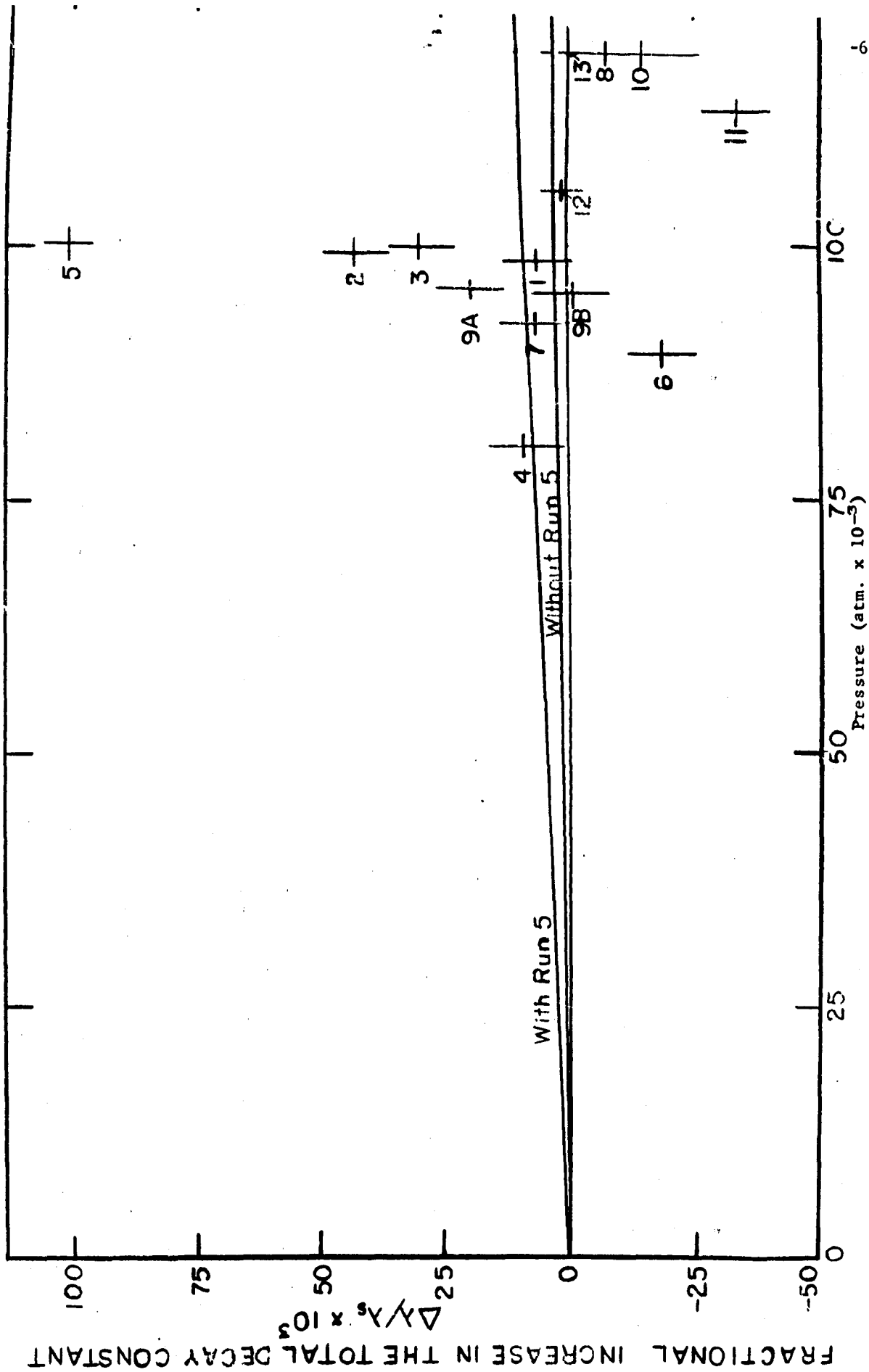


FIG. 6. FRACTIONAL INCREASE IN THE TOTAL DECAY CONSTANT WITH PRESSURE FOR BERYLLIUM (7) IN THE LEAD-MODIFIED TYPE II PRESSURE CELL

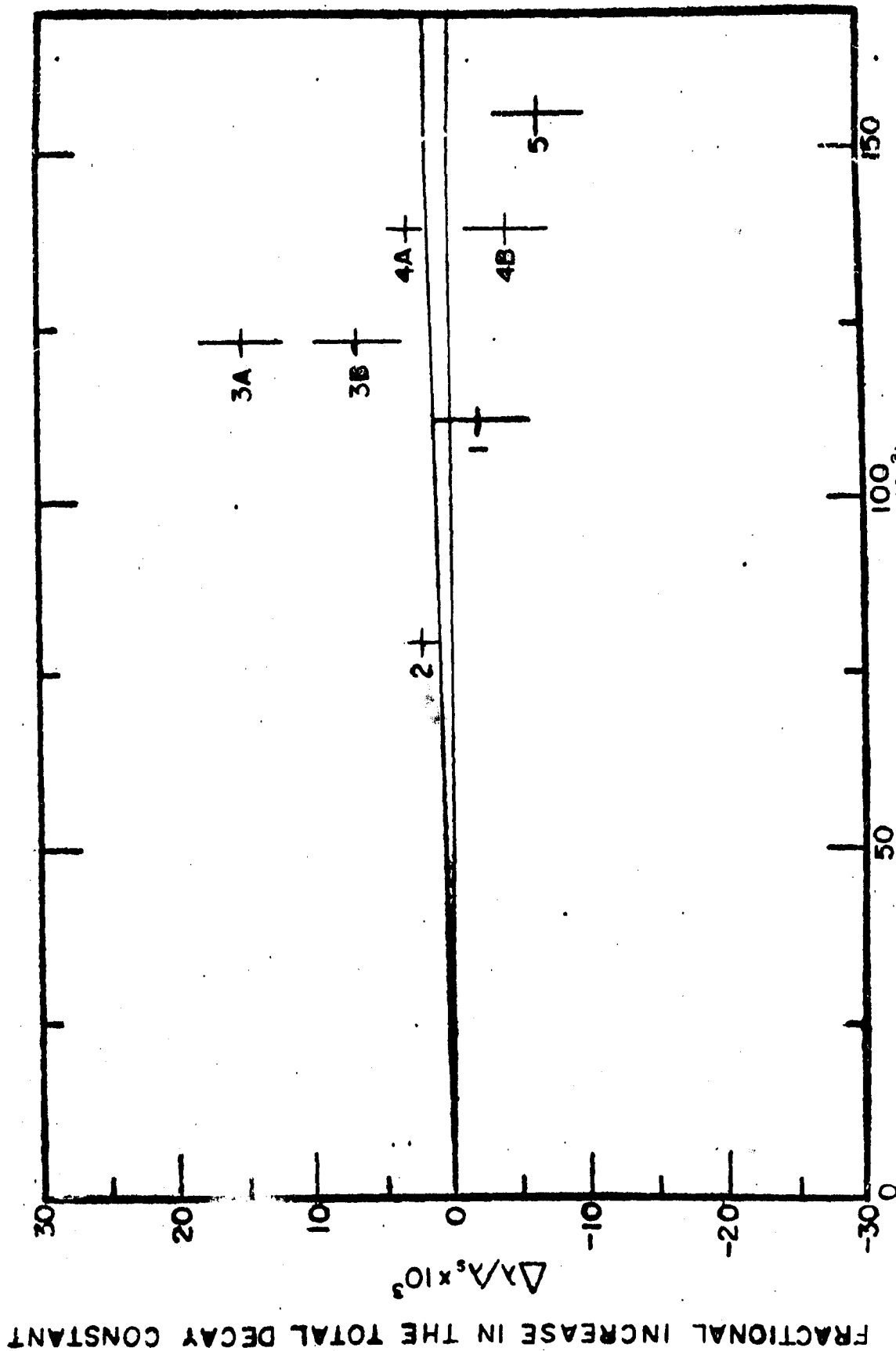


FIG. 7. FRACTIONAL INCREASE IN THE TOTAL DECAY CONSTANT WITH AVERAGE PRESSURE FOR BERYLLIUM (7) IN THE TYPE I PRESSURE CELL

FRACTIONAL INCREASE IN THE TOTAL DECAY CONSTANT

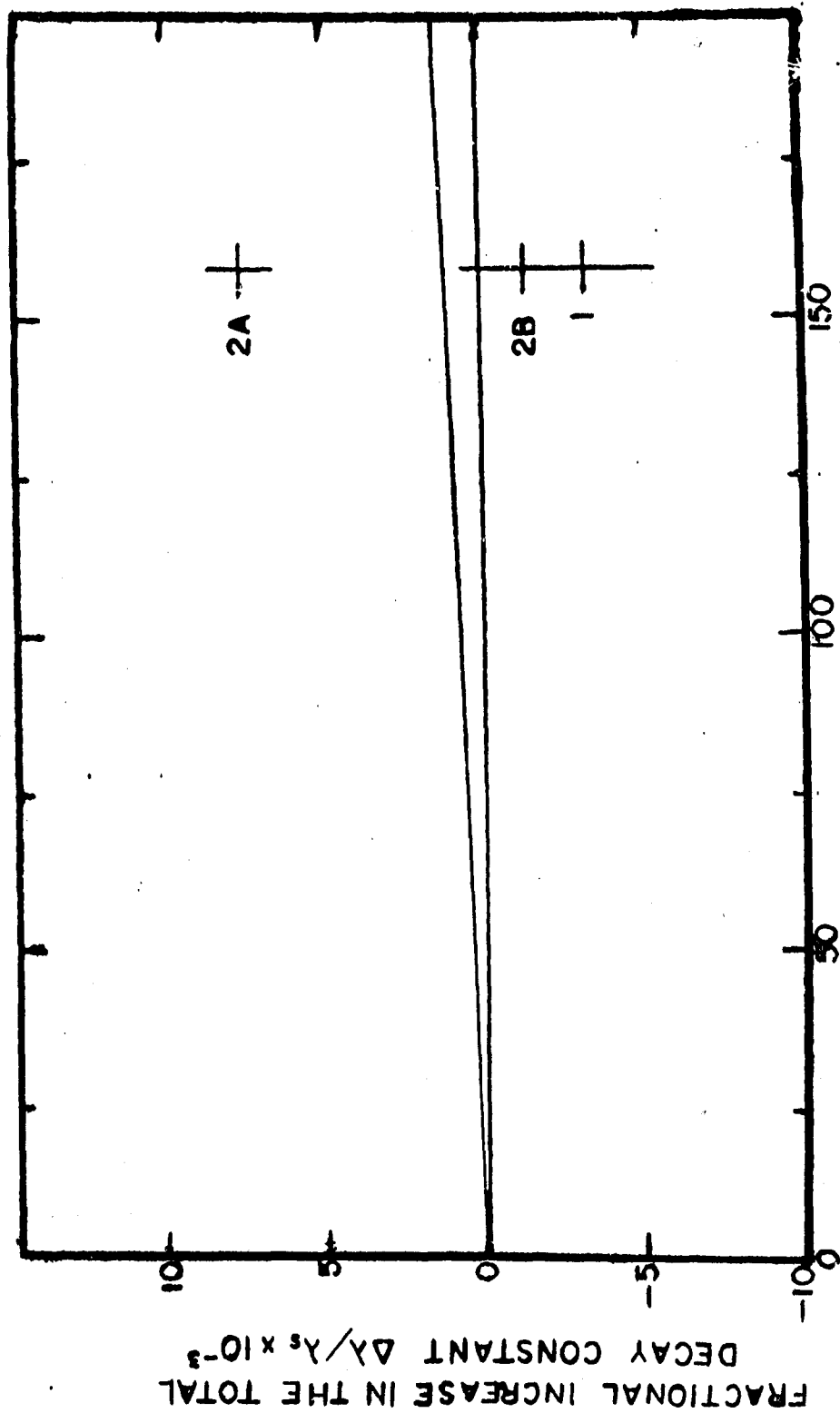


FIG. 8 . FRACTIONAL INCREASE IN THE TOTAL DECAY CONSTANT WITH PRESSURE FOR BARIUM (131) IN THE SILVER-CHLORIDE-MODIFIED TYPE II PRESSURE CELL

LITERATURE CITED

1. Benoist, P., R. Bouchez, P. Daudel, R. Daudel, and A. Rogozinski, Phys. Rev., 76, 1000 (1949).
2. Bouchez, R., P. Daudel, R. Daudel, and R. Muxart, J. Phys. Radium, 8, 336 (1947).
3. Bouchez, R., P. Daudel, R. Daudel, and R. Muxart, Compt. Rend., 227, 525 (1948).
4. Bouchez, R., P. Daudel, R. Daudel, R. Muxart, and A. Rogozinski, J. Phys. Radium, 10, 201 (1949).
5. Bridgman, P. W., Phys. Rev., 60, 351 (1941).
6. Chem. Eng. News 30, 654 (1952).
7. Daudel, R., Rev. Sci., 85, 162 (1947).
8. Gogarty, W. B., S. S. Kistler, and E. B. Christiansen, J. Am Ceram. Soc., 45 [4], (1962).
9. Gogarty, W. B., Ph.D. Thesis, University of Utah (1960).
10. Gogarty, W. B., S. S. Kistler, and E. B. Christiansen, Rev. Sci. Instr., 32, 775 (1961).
11. Kraushaar, J. J., E. D. Wilson, and K. T. Bainbridge, Phys. Rev., 90, 610 (1953).
12. Leininger, R. F., E. Segre, and C. E. Wiegand, Phys. Rev., 76, 897 (1949).
13. Leininger, R. F., E. Segre, and C. E. Wiegand, Phys. Rev., 81, 280 (1951).
14. Porter, R. A. and W. G. McMillan, Phys. Rev., 117, 795 (1960).
15. Segre, E., Phys. Rev., 71, 274 (1947).
16. Segre, E. and C. E. Wiegand, Phys. Rev., 75, 39 (1949).
17. Segre, E. and C. E. Wiegand, Phys. Rev., 81, 284 (1951).
18. Strominger, D., J. M. Hollander, and G. T. Seaborg, Revs. Modern Phys., 30, 585 (1958).

TECHNICAL REPORT DISTRIBUTION LIST

University of Utah

Contract Nonr 1288(02)Project NR-052-357

<u>Addressee</u>	<u>No. Copies Sent</u>	<u>Addressee</u>	<u>No. Copies Sent</u>
Commanding Officer Office of Naval Research Branch Office The John Crear Library Building 86 East Randolph Street Chicago 1, Illinois	(1)	Scientific Director Quartermaster Research and Development Command Natick, Massachusetts	(1)
Commanding Officer Office of Naval Research Branch Office 346 Broadway New York 13, New York	(1)	Director Office of Scientific Research Air Research and Development Command Washington 25, D. C.	(1)
Commanding Officer Office of Naval Research Branch Office 1030 East Green Street Pasadena 1, California	(1)	Commanding Officer Diamond Ordnance Fuze Laboratories Washington 25, D. C. Attn: Technical Reference Section (ORDTL 06.33)	(1)
Commanding Officer Office of Naval Research Branch Office Navy #100 Fleet Post Office New York, New York	(7)	Office of Chief of Staff (R and D) Department of the Army Pentagon 3B516 Washington 25, D. C. Attn: Chemical Advisor	(1)
Director Naval Research Laboratory Washington 25, D. C. Attn: Technical Information Officer	(6)	Chief, Bureau of Ships Department of the Navy Washington 25, D. C. Attn: Code 331	(2)
Chief of Naval Research Washington 25, D. C. Attn: Code 425	(2)	Chief, Bureau of Aeronautics Department of the Navy Washington 25, D. C. Attn: Code TD-4	(2)
Technical Library OASD (R and D) Pentagon Room 3E1065 Washington 25, D. C.	(1)	Chief, Bureau of Ordnance Department of the Navy Washington 25, D. C. Attn: Code Ad-3	(2)
Technical Director Research and Development Division Office of the Quartermaster General Department of the Army Washington 25, D. C.	(1)	ASTIA Document Service Center Arlington Hall Station Arlington 12, Virginia	(5)
Research Director Chemical and Plastics Division Quartermaster Research and Development Command Natick, Massachusetts	(1)	Institute of Geophysics University of California Los Angeles 24, California Attn: Dr. D. T. Griggs	(1)

TECHNICAL REPORT DISTRIBUTION LIST

(continued)

<u>Addressee</u>	<u>No. Copies Sent</u>	<u>Addressee</u>	<u>No. Copies Sent</u>
Univ. of Utah Nonr 1288(02) NR-052-357			
Director of Research Signal Corps Eng'g Laboratories Fort Monmouth, New Jersey	(1)	Commanding Officer Office of Naval Research Branch Office 1000 Geary Street San Francisco 9, California	(2)
Naval Radiological Defense Lab. San Francisco 24, California Attn: Technical Library	(1)	Chief of Naval Research Department of the Navy Washington 25, D. C. Attn: Code 423	(1)
Naval Ordnance Test Station China Lake, California Attn: Head, Chemistry Division	(1)	Dr. Carl J. Christensen, Director Cooperative Research University of Utah Salt Lake City 12, Utah	(1)
Commanding Officer Office of Ordnance Research Box M, Duke Station Durham, North Carolina	(1)	Dr. S. Young Tyree, Jr. Department of Chemistry University of North Carolina Chapel Hill, North Carolina	(1)
U. S. Army Chemical Warfare Laboratories Technical Library Army Chemical Center, Maryland	(1)	Dr. S. Zerfoss Refractories Division National Bureau of Standards Washington 25, D. C.	(1)
Brookhaven National Laboratory Chemistry Division Upton, New York	(1)	Dr. H. Tracy Hall Brigham Young University Provo, Utah	(1)
Atomic Energy Commission Research Division, Chemistry Branch Washington 25, D. C.	(1)	Dr. Francis Birch Department of Geology Harvard University Cambridge, Massachusetts	(1)
Atomic Energy Commission Library Branch Technical Information ORE Post Office Box E Oak Ridge, Tennessee	(1)	Dr. G. Barth-Wehrenalp Pennsalt Chemicals Corporation P. O. Box 4388 Philadelphia 18, Pennsylvania	(2)
Office of Technical Services Department of Commerce Washington 25, D. C.	(1)	Engineering Library University of Utah Salt Lake City 12, Utah	(12)
Dr. W. J. Kirkpatrick Mellon Institute Pittsburgh, Pennsylvania	(1)		
College of Mineral Industries Pennsylvania State College State College, Pennsylvania Attn: Dr. O. F. Tuttle	(1)		